CHALMERS
UNIVERSITY OF TECHNOLOGY

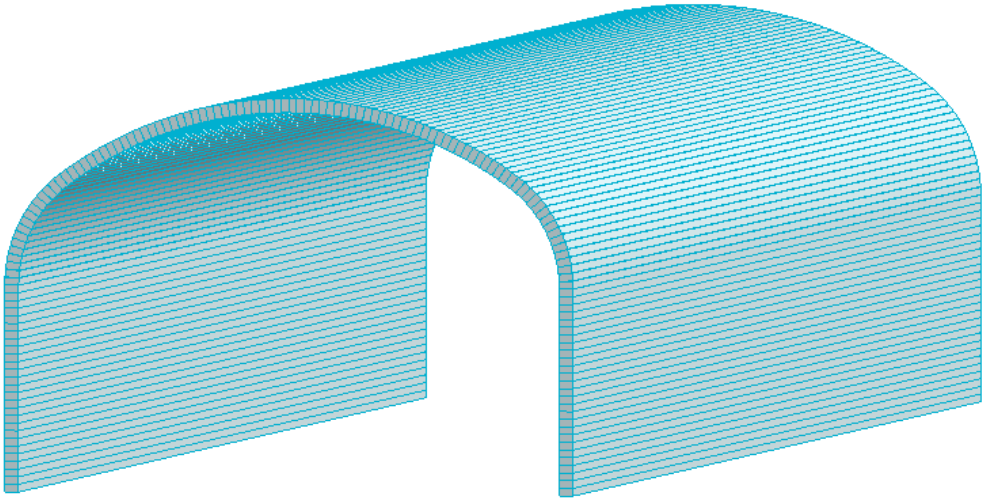

Investigation of textile reinforced concrete in tunnel linings

Master's thesis in ACEX30

THERESE NILSSON
HANNA SEGERHOLM

DEPARTMENT OF ARCHITECTURE AND CIVIL ENGINEERING

CHALMERS UNIVERSITY OF TECHNOLOGY
Gothenburg, Sweden 2025
www.chalmers.se

Master's thesis 2025

Investigation of textile reinforced concrete in tunnel linings

THERESE NILSSON
HANNA SEGERHOLM

CHALMERS
UNIVERSITY OF TECHNOLOGY

Department of Architecture and Civil engineering
Division of Structural engineering and building technology
Chalmers University of Technology
Gothenburg, Sweden 2025

Investigation of textile reinforced concrete in tunnel linings
THERESE NILSSON, HANNA SEGERHOLM

Supervisor:
Valbona Mara, AFRY
Gabriel Edefors, Department of Architecture and Civil engineering
Examiner:
Karin Lundgren, Department of Architecture and Civil engineering

Master's Thesis 2025
Department of Architecture and Civil engineering
Division of Structural engineering and building technology
Chalmers University of Technology
SE-412 96 Gothenburg
Telephone +46 31 772 1000

Cover: Model of tunnel lining visualized in FEM-design 24

Typeset in LaTeX
Printed by Chalmers Reproservice
Gothenburg, Sweden 2025

Investigation of textile reinforced concrete in tunnel linings
THERESE NILSSON
HANNA SEGERHOLM
Department of Architecture and Civil engineering
Chalmers University of Technology

Abstract

This thesis investigates the feasibility and potential advantages of using textile reinforced concrete (TRC) in tunnel linings compared to conventional steel reinforced concrete (RC). The study evaluates structural performance, durability, and environmental impact by combining a detailed literature review with a case study involving finite element modelling of a tunnel lining. By designing a cross-section for each material, a structural comparison of RC and TRC lining was made, as well as a comparison of CO_2-eq emission. TRC, utilizing non-corrosive carbon fibre meshes and high-strength fine-grained concrete, allows for significantly thinner structural elements due to the elimination of concrete cover requirements. Findings of this thesis indicate that TRC linings can achieve equivalent structural performance with reduced material usage and environmental impact. However, limitations regarding fire resistance, especially concerning the behaviour of resin-impregnated textiles under high temperatures, highlight the need for further research. The thesis concludes that TRC is a promising alternative for tunnel lining applications, particularly in non-load-bearing scenarios or where design flexibility and sustainability are prioritized.

Keywords: textile reinforced concrete, tunnel lining, carbon textile mesh, carbon fibres, epoxy resin, textile mesh, textile reinforcement, sustainability.

Acknowledgements

First and foremost, we would like to express our gratitude to our supervisors at AFRY, Valbona Mara and at Chalmers, Gabriel Edefors. A big thank you for your guidance and support throughout the entire project, and for always taking your time from your schedules to assist us. A sincere thank you to our examiner Karin Lundgren for your useful input in the content of this report and taking time and effort to support our work. We would also like to thank Torsten Knobloch from Solidian Kelteks for his valuable knowledge on the material parameters of TRC. Thank you gmp Architects for the permission to use the picture of Hypar Shell, seen in Figure 2.8, and thank you Solidian Kelteks for the permission to use pictures of Albstadt-Lautlingen bridge and Albstadt-Ebingen bridge, seen in Figure 2.9 and Figure 2.10.

Therese Nilsson, Hanna Segerholm, Gothenburg, June 2025

List of Acronyms

Below is the list of acronyms that have been used throughout this thesis listed in alphabetical order:

AR-glass	Alkali resistant glass
BF	Basalt fiber
CF	Carbon fiber
FRC	Fibre reinforced concrete
FRP	Fibre reinforced polymer
GF	Glass fiber
PP	Polypropylene
RC	Conventional reinforced concrete (steel)
TRC	Textile reinforced concrete

Contents

List of Figures

List of Tables

1 Introduction

Exploring and analysing new building materials and techniques is essential to keep developing the building industry and finding new sustainable and more optimized solutions. An example of a rather new material is textile reinforced concrete (TRC) which utilizes the combination of a corrosion-resistant reinforcement and high strength concrete.

1.1 Background

Today, steel reinforced concrete (RC) is the most widely used construction material in the world (Chahar and Pal, 2022). Although steel bars are the universal solution for reinforcement in concrete, their susceptibility to corrosion has prompted the exploration of alternative solutions, such as textile reinforcement. In order to protect the corrosive steel bars in RC, a thick concrete cover is needed. In contrast, for TRC, this is not required in terms of chloride protection, enabling a thinner concrete cover. The reduction of concrete can create a more slender profile, and a more sustainable construction. It can lead to a reduced need for maintenance and repair, which in turn can lead to lower long-term costs and, in general, a longer lifespan compared to RC. Additionally, the reduction of concrete can result in lower net CO_2-eq emissions.

Furthermore, a significant quality of TRC is its high flexibility and formability. This characteristic is beneficial when producing structures with complex geometry, such as curve- and shell-shaped components (Peled et al., 2017). TRC is also beneficial to use when designing lightweight structures, as it has a low weight in relation to its load capacity. These abilities make TRC an advantageous material to use when, for example, constructing tunnel linings.

In Sweden the use of concrete tunnel linings is limited, however, it occurs in some places as a cladding and as a water and frost protection. This type of structure has low maintenance during its service life as it is part of the tunnel itself. Using TRC in tunnel linings has not been done before, however, the material is potentially beneficial due to its flexible nature and possibility to thin structures.

1.2 Aim and objectives

The aim of this master thesis was to analyse the behaviour of TRC and its use in existing projects. Furthermore, analysing the possibility of using it in tunnel linings and the potential benefits of exchanging RC with TRC in such structures. Consequently, the objectives of this master thesis were the following:

- Conduct a literature study on the material properties and behaviour of TRC. The study should also address the functional requirements and design loads

relevant to tunnel linings. Additionally, evaluate the potential use of TRC in tunnel lining applications.
- Design two tunnel linings with an optimized cross-section, one using RC and one using TRC.
- Conduct a comparison between the two tunnel lining designs, with regard to height of chosen cross-section, amount of concrete used, and estimated net CO_2-eq emissions.

1.3 Methodology

The project was divided into two main parts, a literature study and a case study comparing one tunnel lining made of TRC and one using RC. Detailed information on the different parts will be presented in the following sections.

1.3.1 Literature study

The theoretical study was conducted by an investigation of textile reinforcement and TRC including the material properties and their behaviour. Further on, a study of TRC used in existing projects and the possibility to use in tunnel linings was done. This was done to get a deeper understanding of the subject in order to qualitatively compare TRC with RC, as well as draw conclusions of which material performs better in regard to tunnel linings and its requirements.

1.3.2 Case study

The case study was carried out by developing a model of a tunnel lining to design one with RC and one with TRC. The model was created in FEM design 24 (version 24.00.002) using the API plug-in software program Grasshopper (version Tuesday, 11 June 2024), as it provides parametric inputs. For the numerical analysis, relevant material parameters and properties were gathered. The case study was used as a complement to the literature study to investigate potential similarities and differences between the two materials, as well as to quantify the possible savings of using TRC. Furthermore, if it is environmentally justifiable to replace RC with TRC in tunnel linings. The results of the modelling were validated through analytical calculations.

1.4 Limitations

The case study did not include different material combinations of TRC, only carbon fibres where considered. Therefore, the literature study was primarily focused on carbon fibres. Furthermore, the analysis did not contain any calculations that included creep, shrinkage, or fatigue for concrete. However, fatigue behaviour was acknowledged in the literature study and a simplified model of shrinkage was conducted with regard to calculations of crack width for RC. Furthermore, some requirements

and loads mentioned in this report regarding tunnel linings were not accounted for in the case study. A more detailed limitation is presented in relevant chapter.

The CO_2-eq calculations in this report were simplified in the sense that only the production of the materials was considered.

2 Textile reinforced concrete (TRC)

For the literature study, a deeper understanding of the materials was obtained in order to do a qualitative comparison between RC and TRC in tunnel linings. In this chapter, the composition, behaviour and existing application of TRC as well as the use of TRC in tunnel linings are described.

2.1 Composition of TRC

TRC is a composite material that is fabricated of a concrete mix and non-corrosive textile. It follows the same principles as RC, where the concrete has a high compressive strength and the reinforcement has a high tensile capacity (Friese et al., 2022). By using a fine-grained concrete reinforced with textile yarns from long continuous fibres, also called filaments, TRC is combined. The non-corrosive textile opens up opportunities to create thin-structured and lightweight concrete elements. The high fibre strength, flexibility in bending, and stiffness in tension allow for the possibilities of geometry and suitability for curved structures to broaden (Friese et al., 2022). In the following chapter, the components of TRC will be described.

2.1.1 Concrete

Concrete can simply be described as a compound material that consists of aggregates and a binding medium, typically hydraulic cement and water. However, for TRC, the mixture differs from conventional concrete. The aggregate size is limited and has to be considerably smaller, typically less than 2 mm (Williams Portal, 2015). However, a small aggregate size results in a large quantity of cement paste, and therefore a slightly larger aggregate size, 4-6 mm, can also be considered. The need for this requirement is for the concrete mix to be flowable enough to penetrate the textile reinforcement since the openings in the grid and the distance between the layers are small, see Chapter 2.1.2 Textile. It is of high importance for the concrete matrix to fully fill the empty space in the textile for the bond and load transfer from the concrete to the reinforcement to operate. The small size of aggregates leads to a matrix in which the properties correspond to high-strength concrete, however, with an appearance closer to mortar (Hartig, 2011).

Another important aspect is for the concrete matrix to be chemically compatible with the reinforcement e.g. alkalinity when working with glass fibres. A high alkalinity can lead to a degradation of the glass filaments and therefore it is preferred to use a binder with a low amount of Portland cement (Hartig, 2011).

2.1.2 Textile

For TRC, textile reinforcement is made of filaments bunched into yarns/rovings that are then woven into an open mesh or grid pattern (Williams Portal et al., n.d.). The

filaments are made of fibres and there are two categories that fibres are usually divided into: natural and man-made. Fibres made from geological processes, plants, and animals are categorized into natural fibres while fibres made from inorganic and synthetic materials are categorized into man-made fibres (Peled et al., 2017). Of the man-made fibres, glass fibres (GF), carbon fibres (CF), and basalt fibres (BF) are the three essential types of fibre used as reinforcement for concrete (Friese et al., 2022). Depending on the fibres origin, different production methods are used. For a reinforcing purpose, long continuous fibres (filaments) are preferred, and these filaments are then bundled up together, anything from hundreds to thousands, to create yarns/rovings (Brameshuber and Brockmann, 2006).

The yarns are used to create a mesh where different textile fabrication methods can be used. The yarns that are placed along the length of the textile are called warp and those along the width are called weft (Peled et al., 2017). The size of the grid opening differs from case to case, however it is crucial that it is larger than the largest aggregate size in the concrete matrix, which is mentioned in Chapter 2.1.1 Concrete. An example of a mesh with warp 4.8 mm with space 33.5 mm and weft 5.5 mm with space 32.8 mm, can be seen in Figure 2.1.

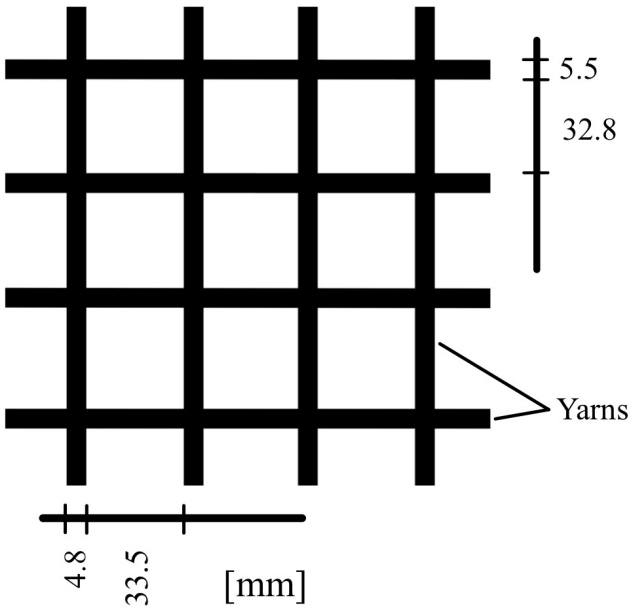

Figure 2.1: Example of a textile mesh (solidian GmbH, 2024).

By using meshes in TRC, the textile fibres can be oriented in the direction of the maximum tensile stresses to optimize their full capacity, since it has a significant effect on the load carrying capacity (Brameshuber and Brockmann, 2006). The amount of layers of meshes in TRC also contributes to the load capacity where an increase of layers have an increase in load capacity (Blomqvist, 2021).

In contrast, another arrangement exists called fibre reinforced concrete (FRC), where short fibres are mixed in the concrete and therefore, placed irregularly. This results

in the utilization rate of the individual fibres to vary since some will be placed parallel and others perpendicular to the load direction. The arrangement of the textile mesh in TRC is more similar to the arrangement of steel bars in RC compared to FRC. The orientation of the reinforcement for RC, FRC, and TRC can be seen in Figure 2.2.

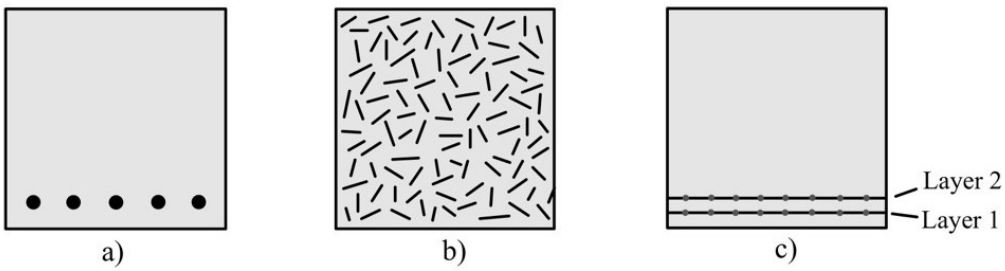

Figure 2.2: Distribution and alignment of reinforcement in a) RC, b) FRC, c) TRC

2.2 Behaviour of TRC

Since TRC is a composite material, the behaviour of TRC depends on the material characteristics itself but also on the interaction between the concrete and textile reinforcement (Williams Portal et al., n.d.). In the following chapter the behaviour of TRC is therefore described in terms of load-bearing, fire, and fatigue behaviour as well as its interaction, bond behaviour.

2.2.1 Load-bearing behaviour

The bond behaviour in TRC has a significant influence on the load-bearing behaviour (Brameshuber and Brockmann, 2006). To analyse the load-bearing behaviour, a stress-strain curve from uniaxial loading can be studied. The curve from TRC can be divided into three sections, state I, II and III, a characteristic also commonly recognized in RC. This behaviour corresponds to that of RC with the exception of state III, see Figure 2.3.

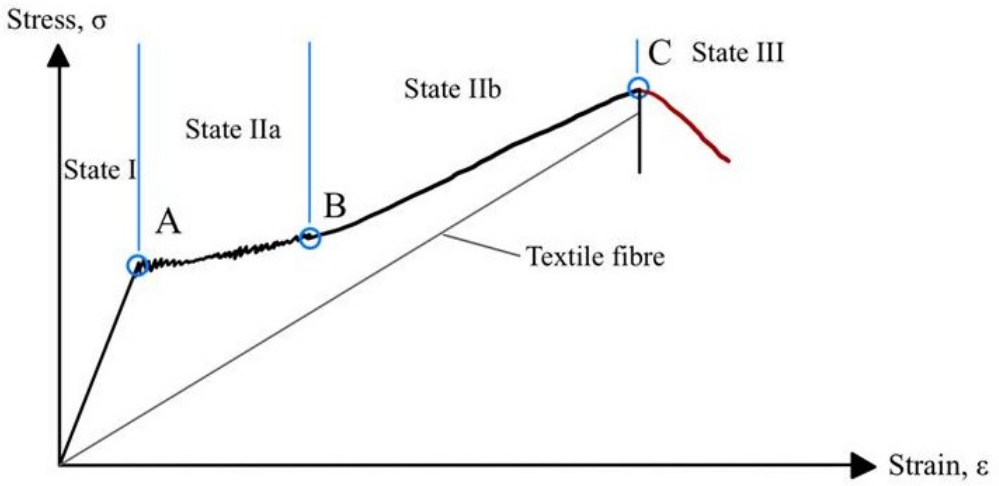

Figure 2.3: Stress-strain curve of TRC (black line) and RC (red line)

State I:
At the start of loading, the concrete is uncracked and the material is linear-elastic (Brameshuber and Brockmann, 2006). The E-modulus of TRC corresponds nearly to the E-modulus of the concrete matrix.

State IIa:
Once the concrete tensile strength is exceeded, the first crack appears, see point A in Figure 2.3 (Brameshuber and Brockmann, 2006). At this stage, the entire tensile force within the crack is carried by the mesh. The mesh must resist the acting load or the composite fails. As the tension force increases, more cracks occur. Forces in the concrete are initiated due to the bond between filaments and concrete until the tensile strength of the concrete is reached once more. The crack spacing and width depend on the mesh properties, the bonding between the mesh and the concrete matrix, as well as the concrete matrix's tensile failure strain. During state IIa, the stress-strain curve exhibits only a minimal increase.

State IIb:
In this stage, no further cracks occur (stabilized crack pattern) (Brameshuber and Brockmann, 2006). With increasing load, the filaments are strained up until they reach their ultimate strength. The stress-strain curve in this stage runs almost parallel to that of pure textile.

State III:
Due to its textile reinforcement, TRC will not have ductile deformation as these materials do not have plastic capacity (Brameshuber and Brockmann, 2006). Consequently, TRC fails in a brittle manner upon reaching the tensile failure strain of the mesh. The difference in state III between TRC and RC is shown in Figure 2.3.

2.2.2 Bond behaviour

The bond behaviour differs from that of RC since the filaments have an heterogenous cross-section in contrast to steel. The bond behaviour in TRC is not only between the filaments and the cement but also between the filaments themselves. The force transmission between the concrete and the textile is via adhesion and friction (Hartig, 2011). However, the load transfer between the filaments in the yarn/roving is based on either adhesion or friction which depends on the quality of the bond between the filaments (Williams Portal et al., n.d.).

For this interaction to be possible it is important that the matrix can fully penetrate the textile mesh. It is also of great importance for no displacements of the threads, when casting the concrete, to maintain the required bond (Peled et al., 2017).

The filaments are usually divided up into two groups, outer filaments and inner filaments. The outer filaments, also called sleeve filaments, are embedded in the hardened cement, while the inner filaments, also called core filaments, have no direct contact. Figure 2.4 shows how the inner and outer filaments in the concrete are arranged.

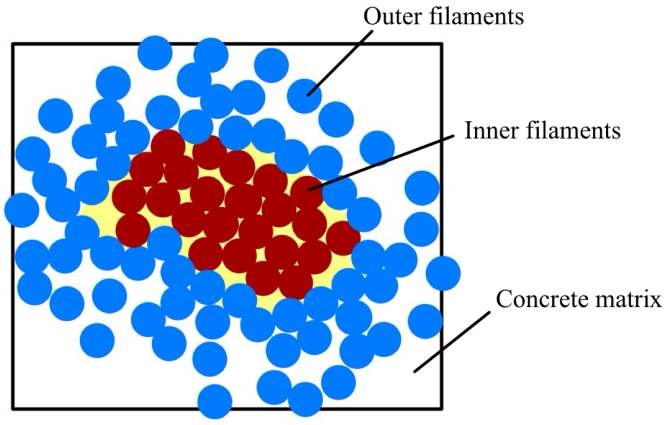

Figure 2.4: Arrangement of outer and inner filaments

The sleeve filaments have better bond performance, compared to the core filaments, due to having good anchorage in the concrete matrix since they are embedded in the hardened cement (Brameshuber and Brockmann, 2006). The core filaments are not in direct contact with the concrete matrix and therefore only stressed indirectly by the sleeve filaments. The core filaments can therefore slip easily and create friction since they are not anchored in the concrete matrix. A bond resistance can be caused by this friction within the yarn/rowings. An impregnation can be used on the filaments, resulting in a more rigid composition. The core filaments therefore no longer slip within the sleeve filaments and allow the whole filaments to be anchored in the hardened cement. The impregnation also results in the filaments receiving a

homogeneous yarn structure.

The bond-slip behaviour is crucial to understand the global structural behaviour (Williams Portal, 2015). The bond-slip behaviour of RC can be seen in Figure 2.5.

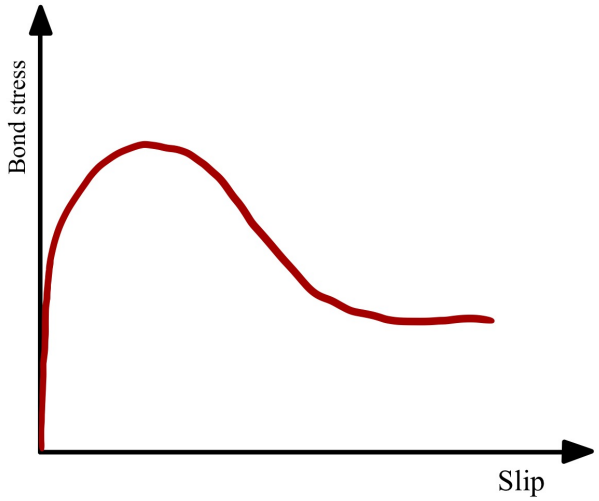

Figure 2.5: Bond slip behaviour for RC

As mentioned earlier, an important factor for the bond-slip behaviour of TRC is the effect of using an impregnation. By using an impregnation, the internal bond can be changed (Brameshuber and Brockmann, 2006). The inner bond becomes larger than the outer bond and the yarn can be seen as a composite material made of the filaments and the resin. In contrast to this, when not using an impregnation this results in the core filaments to be able to slip with respect to the sleeve filaments. This means that the inner bond is smaller than the outer bond. The relation between the inner and outer bond affects the bond slip behaviour of the reinforcement. If the internal bond is weak, the material can be weak but ductile. However, if the internal bond is strong, the material can be strong but brittle. By having the yarns impregnated and therefore creating a stronger internal bond, the material can reach higher load capacities and higher resistance against slip. This, however, leads to the ductility to be low since after a certain slip occurs, all filaments fail at almost the exact same time. In contrast, when the yarns are not impregnated the load capacity is lower but the ductility much larger. This is due to the higher slippage of the inner filaments inside the yarns. The slippage leads to different stresses in the filaments and results in a successive failure rather than a brittle, see Figure 2.6.

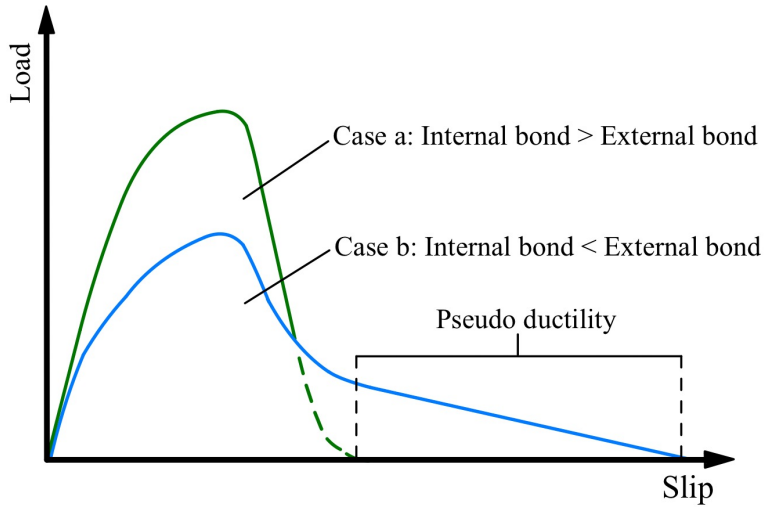

Figure 2.6: Bond slip behaviour for impregnated yarns (Case a) vs non impregnated yarns (Case b)

2.2.3 Fire resistance

Since TRC structures have a small concrete cover, it is necessary to take into account the ability to resist high temperatures, if exposed to fire. This is because thinner concrete covers results in worse fire protection since the temperature in the structure rises quicker (Van Coile et al., 2011). Fire resistance is also important to consider when designing tunnels. It is important to consider both the fire performance and the fire resistance of the textile, concrete, and the composite of TRC.

When investigating the fire behaviour of textiles in TRC it is mainly the tensile strength at higher temperatures and the thermal coefficient that are of importance. The tensile strength of the textile varies depending on which type of fibre the textile is made of. Between glass fibres, aramid fibres and carbon fibres, the most common carbon fibres can resist the highest temperatures where the tensile strength start to decrease slightly when the temperature is up to 900°C compared to over 400°C for glass fibres (Brameshuber and Brockmann, 2006). The tensile behaviour is also different between different types of fibres. At high temperatures, carbon fibres and aramid fibres carbonize and/or decompose, whereas glass fibres have a similar behaviour as steel reinforcement and melt at high temperatures.

The axial coefficient of thermal expansion is -0.4×10^{-6} K^{-1} for carbon fibres (Brameshuber and Brockmann, 2006). Carbon fibres therefore become shorter when the temperature increases as the axial coefficient of thermal expansion is negative in room temperature. Since the axial coefficient of thermal expansion for fine grained concrete with high strength is around $14{\times}10^{-6}$ to $20{\times}10^{-6}$ K^{-1} it results in constrained stresses. The different thermal coefficients between carbon fibres and fine grained concrete lead to compressive stresses in the concrete and tension in the fibres.

As mentioned, high temperatures can lead to constraint stresses and these can cause micro cracking which results in the microstructure starting to deteriorate. For conventional concrete, micro cracking starts when the temperature is around 150°C and increases rapidly around 450°C. However, for fine grained concrete, micro cracking is expected to be small (Brameshuber and Brockmann, 2006). This is because fine grained concrete has a high binder content, small aggregate size, and low pore volume.

Another mechanism that can occur in the concrete is spalling. This is because when the temperature increases, the water in the concrete vaporizes and changes the hydrated cement structure. When the temperature is 100°C, vapour is formed from the free water and can cause vapour pressure. If the concrete tensile strength is lower than the vapour pressure, concrete spalling occurs. For concretes with low porosity, as a fine-grained concrete, the risk of spalling is smaller (Korten and Wetzig, 2013). The low porosity leads to less water content in the pores which results in a lower water pressure when heating the concrete. A thinner specimen of concrete also leads to a lower risk to spalling due to it having a faster crack formation. The cracks result in the vapour escaping and therefore the faster crack formation the faster decrease of vapour pressure.

One way to minimize the risk of concrete spalling is to use polypropylene (PP) fibres (Suiffi et al., 2021). PP fibres melt around 160 °C and form micro-channels. The vapour that is formed in the concrete can therefore transfer through the micro-channels and escape, reducing the risk of spalling. A study done investigated the effect on PP fibres in concrete when exposed to elevated temperatures at 200°C, 400°C and 600°C for 2, 4 and 6 hours (Shihada, 2011). The compressive strength in room temperature for 0%, 0.5% and 1.0% PP-fibres were 32 MPa, 36 MPa, and 38 MPa, respectively. The study showed that an optimal amount of PP fibres is around 0.5% of the total volume as it decreased the loss of compressive strength for all temperatures compared to the samples with 0% PP-fibres. The loss of compressive strength for 0% PP-fibres were 16.93% - 41.34% depending on temperature and duration. For 0.5% PP fibres, the samples had a loss of compressive strength at 8.08% - 20.41%. The samples with 1.0% PP fibres had a larger loss of compressive strength for almost every temperature and duration, however, the compressive strength was still higher after exposed to elevated temperatures compared to the samples with 0%. The compressive strength for the samples with 1.0% PP-fibres had a loss of 20.57% - 43.26%.

In TRC, the use of resin can improve the bond between the textile and concrete, as well as increase the tensile strength. However, if a coating is applied it is of importance to consider its fire behaviour. Most resins have a worse fire behaviour than both concrete and textiles and decompose at lower temperatures (Brameshuber and Brockmann, 2006). This results in bond failure at low temperatures which in turn lead to element failure. For epoxy resin, it starts to decompose at 120 °C if exposed to the heat for 90 minutes (Xu et al., 2014). The decomposition of resin that results in a loss of bond strength can also increase the risk of spalling (Fürst et al., 2022).

However, there are some resins that are optimized for higher temperatures, which might contribute to improved fire behaviour. These have been studied but requires to be tested further.

In a study conducted, the bond behaviour of mineral impregnated and polymer impregnated carbon fibres was compared at high temperatures by performing a pull-out test after heating (Schneider et al., 2018). They were heated up to 500°C for up to 1.5 hours. The result of this study was that the specimens with mineral impregnation showed excellent values in terms of bond modulus, maximum extraction force, and post-failure behaviour. While the polymer impregnated specimens showed a loss of bond strength of 80% at temperatures of 200°C, the mineral impregnation showed only a loss of 65% at 500°C. The mineral impregnation matrix was able to demonstrate good performance even at elevated temperatures due to its high transverse stiffness. The bond strength of the polymer impregnated specimens is dependent on form closure effects. This form closure can no longer transfer stresses at higher temperatures, and with the softening of the polymer impregnation, the bond strength decreases significantly.

A detail worth mentioning is that mineral impregnated carbon fibres have a lower tensile strength than polymer impregnated carbon fibres when compared in room temperature (Silva et al., 2022). While cement-based mineral impregnated carbon fibres have a tensile strength of 1373 MPa, polymer impregnated carbon fibres shows a tensile strength of approximately 2500 MPa.

It is obvious that there are several factors that affect the fire behaviour and fire resistance of TRC. The main issue is the impregnation of the fibres needed for the bond strength. The polymer impregnation that provides high bond strength at room temperature, such as epoxy resin, deteriorates at rather low temperatures with regard to fire. However, the mineral impregnations that are able to withstand higher temperatures have a significantly lower tensile strength, compared to the polymer impregnation. Still, the mineral impregnation shows rather high tensile strength when compared to average steel reinforcement. The fire resistance of impregnated fibres could possibly be improved with further research.

2.2.4 Fatigue behaviour

For structures, exposed to cyclic loads, the strength can decrease over time and cause fatigue problems (Kachkouch et al., 2022). For tunnels, fatigue is an important aspect to consider because the air pressure and suction generated from train traffic acts as a cyclic load.

Fatigue behaviour can be analysed for two types of fatigue loading, causing different failure characteristics (Ahsan, n.d.). One in which the load is applied with high numbers of cycles at lower stress levels (high cycle), and one in which the load is applied with lower number of cycles at high stress levels (low cycle). The suction and pressure load from trains in tunnels is considered as high cycle fatigue loading.

A study done compared carbon textile reinforced concrete and AR-glass textile reinforced concrete under fatigue loading (Zhu et al., 2024). The specimens had the dimensions 15x30x230mm and were tested for both high cycle fatigue and low cycle fatigue. Before the fatigue tests was carried out, a quasi-static tensile test was done. For the high cycle fatigue, the specimens were loaded at a stress range between 2.5% and 30% of the static tensile strength for up to 10,000 cycles. The investigation showed that the specimen reinforced with carbon textile had more cracks but a more uniform strain distribution through the section compared to AR-glass textile. Carbon textile also had higher tensile reduction compared to AR-glass after high-cycle fatigue loading, however, the tensile strength was still higher compared to AR-glass both before and after the fatigue loading. It also showed that the mesh size of the textile reinforcement does not have a significant impact on the fatigue behaviour, but the textile type and number of layers do. There were 2 failure modes for the carbon textile reinforced concrete; textile pull-out and interlaminar shear failure.

Another study carried out at TU Dresden, Germany, tested epoxy impregnated carbon textile reinforcement with high strength concrete under fatigue loading (Wagner and Curbach, 2019). The study investigated the bond fatigue behaviour of specimens at different load levels and with different anchorage length. The dimensions of the specimens were 110 mm wide and 30 mm thick with various lengths between 76 mm - 304 mm depending on the anchorage lengths. The anchorage lengths were 38 mm, 76 mm, 114 mm and 152 mm. There were 4 specimens tested for every anchorage length and for each load level.

Prior to the cycle-loading a static reference test was performed to determine if the anchorage lengths were sufficient to be further tested. This was done to determine whether the failure was due to textile rupture, indicating that the selected anchorage length was sufficient to fully transfer the tensile load. However, if bond failure occurred, such as the textile being pulled out, the anchorage length was insufficient. The results showed some of the specimens, especially the specimens with anchorage length 38 mm, failing during the static test, and therefore could not be tested further for the cyclic loading.

The specimens were then cycle-loaded with two minimum stresses with different related maximum stresses for up to $2 \cdot 10^6$ cycles. The stresses were specified as a percentage of their reference strength and the two minimum stresses were 30% and 50% and the maximum stress increased after each test series.

The study showed that epoxy impregnated carbon reinforced concrete has good bond fatigue behaviour and the failure of specimens only occurred when the load was applied at the high stress levels, if the anchorage length was not sufficient. Although, high cycle fatigue usually includes applying the load at lower stress levels, the study showed that many of the specimens passed $2 \cdot 10^6$ cycles which is beneficial for using TRC in tunnel linings in terms of fatigue behaviour.

2.2.5 Mechanical properties

The mechanical properties of TRC can vary depending on its composition and the manufacturer. Fine-grained concretes have been specifically developed to achieve optimal compatibility with textile reinforcement. The mechanical properties of certain fine-grained concretes are presented in Table 2.1 (Brameshuber and Brockmann, 2006; Brockmann, 2007).

Table 2.1: Mechanical Properties of fine grained concrete

Material Properties	**Value**
Density [g/cm^3]	2.1 - 2.2
Young's modulus [MPa]	22,000 - 32,000
Compression strength [MPa]	40 - 135
Tensile strength [MPa]	3 - 5
Ultimate strain [%]	0.45 - 0.63

The mechanical properties of carbon fibres varies depending on if the fibres are impregnated or non-impregnated. The mechanical properties, seen in Table 2.2, are taken from a commercially available textile mesh from Solodian Kelteks named GRID Q95-CCE-38 (solidian GmbH, 2024). The textile mesh is made of carbon fibres impregnated with epoxy resin.

Table 2.2: Mechanical Properties of carbon fibre mesh

Material Properties	**Value**
Density [g/cm^3]	1.3
Young's modulus [GPa]	243
Tensile strength [MPa]	1200
Ultimate strain [%]	1.24

2.3 Design for durability

When using TRC, it is also of great importance to consider the durability of the structure and the effect that TRC as a material has on such requirements.

2.3.1 Cracking

When using a non-corrosive reinforcement, such as carbon fibre meshes, the requirements differ from those for steel reinforcement. In SS-EN-1992-1-1:2005 there is a recommended value of the limit crack width when using steel reinforcement, w_{max} = 0.3 mm, for structures with exposure class XC4 and quasi-permanent load combinations, as that for tunnel linings. However, since the reinforcement in TRC is non-corrosive this limit does not have to be applied in the same manner, since the requirement is conducted to reduce the risk of corrosion of steel reinforcement. The cracking pattern for TRC consists of small crack widths and short crack spacing,

and is mainly influenced by the mesh spacing (Williams Portal, 2015). Cracks typically form at every transverse yarn, and due to the small crack spacing, new cracks tend to develop rapidly rather than existing cracks growing significantly (Sciegaj et al., 2023). As of now there are no crack width requirements stated specifically for TRC. In EN 1992-1-1:2023, Annex R9.2, Table R.2, the maximum crack width requirement for fibre reinforced polymer (FRP) reinforcement is $w_{lim,cal}$=0.4 mm. This could possibly be used as a guideline for TRC as well, however it is also stated that this requirement is for appearance only. Since the structure being investigated is inside of a tunnel, this requirement therefore seems to be excessive.

An aspect to consider is that minimizing the crack width for TRC is still important with regard to reducing the ingress of agents that can deteriorate the concrete (Peled et al., 2017). In addition, water ingress into cracks can cause freeze-thaw damage if the water freezes and expands in the cracks. Furthermore, the function of the tunnel lining is to protect the tunnel from water leakage and ice. Therefore, it is of great importance for the tunnel lining to not get through-thickness cracks. However, the application relevant to this report is tunnel linings, which are generally subjected to compressive forces. This compressive state is expected to reduce the risk of through-cracking.

Furthermore, because of the small crack width, TRC has the possibility of crack healing. Crack healing is a natural process in cementitious composites in which microcracks in the concrete close over time (Peled et al., 2017). This is done primarily through the deposition of materials such as calcium carbonate ($CaCO_3$) or continued hydration of unhydrated cement particles within the crack space. Studies has shown that when the cracks are smaller than 100 µm crack healing can take place which is why it is particularly effective in TRC due to the material's ability to control crack widths through a multiple-cracking mechanism. Crack healing has been observed in a test where 20µm cracks showed closing after about one month.

2.3.2 Concrete cover

In SS-EN-1992-1-1:2005 the requirement for concrete cover for steel reinforced concrete is stated and depends on a few variables such as exposure class, diameter of the bars, and concrete strength class. Concrete cover serves several critical functions in RC, including fire protection, corrosion resistance, and ensuring sufficient bond between the steel reinforcement and the surrounding concrete. However, the primary reason for requiring a thicker concrete cover is to reduce the risk of corrosion of the steel bars in RC. For TRC, and specifically carbon fibres, there is no specific requirement. However, in EN-1992-1-1:2023, Annex R.6 (2), it is stated that for embedded FRP reinforcement, unless more accurate information is available based on test data, the concrete cover should be taken as $c_{min,b} \geq 2\phi$ but at least $c_{min,b} \geq 1.5\phi$, however a minimum of 10 mm, where ϕ is the diameter of the FRP bar. This limit can be implemented for TRC due to the concrete cover, which in addition to reducing the risk of corrosion, contributes to fire protection and structural integrity.

2.4 Application of TRC

As of today, there are two main applications of TRC: retrofitting of already existing structures and precast elements of different types, such as façades and bridges. It has been used as a reinforcement of existing building elements as well as on a few bridges, mostly in Germany. This area of use of TRC is rapidly developing and different applications are advancing. In this chapter, some applications that has been done will be further specified along with the possible use of it in tunnel linings.

2.4.1 TRC as strengthening

Recently TRC has been tested and used as a type of additional reinforcement or strengthening on existing structures. It is used as repair and retrofit to extend the life of the element and to improve its performance (Peled et al., 2017). This includes strengthening to compensate for the loss of resistance due to deterioration and ensuring the long-term load-bearing capacity of the existing structures. It can also be used to enhance the mechanical performance of structures to meet new requirements or standards. The application is done by bonding or wrapping the existing elements with layers of impregnated textile around the element with a thickness of 10 to 20 mm. It can be applied on the sides and/or the bottom, or wrapped around the whole component, called jacketing. Its unobtrusive visual is also beneficial for preservation of historical structures.

The first step to strengthen with TRC is to prepare the surface of the relevant concrete member (Sandmann et al., 2023). This involves removing loose material and repairing defects such as cracks and spalling. The surface should also be roughened, usually by high pressure water blasting or sand blasting. The strengthening is then applied by spraying or manual application where the textile is worked into the fresh concrete layer. The textile grids are placed with a spacing of 3 to 5 mm between the layers until the required amount of layers is reached. There are several practical applications that have been done with TRC as strengthening.

An example of an application is the strengthening of a motorway bridge for the A 648 motorway in Germany that was done in 2021 (Sandmann et al., 2023). The prestressed bridge consists of 3 spans and the part of the bridge being strengthened was one of the spans built in 1971 with a service life limited to 2020. When conducting tendon soundings, a testing method for indicating, for instance, corrosion, stress corrosion cracking could not be entirely ruled out. Additionally, re-calculations did not provide sufficient evidence of failure due to deformation or cracking. Therefore, strengthening of the structure was decided. They used uniaxial textile carbon layers together with fine grained concrete. 5 textile layers were placed in the bottom of the edge spans and 6 layers were used in the top of the bridge. For the top layers 2 were placed over the entire span while 4 layers were placed in the support area, see Figure 2.7.

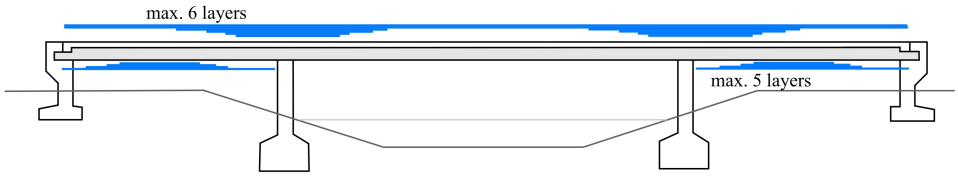

Figure 2.7: Placement of TRC strengthening for motorway bridge

Another example is the repair done on a building called the Hypar Shell in Magdeburg, Germany, which was built in 1969. The structure was constructed with a roof that consists of four hyperbolic paraboloids that span an area of 48x48 m and was designed to be 7 cm thick. However, later it was revealed that the thickness of the roof had been 1 to 2 cm less and the reinforcement had a smaller bar diameter than planned. Furthermore, construction defects during erection of the building as well as weathering during use caused extensive damage to the building, and as a result it had to be closed down in 1997. Conventional repair methods were ruled out mainly due to the high self-weight and in 2017 it was decided that it would be strengthened with carbon textile concrete. It was strengthened with 1 cm thick concrete layers with a grain size of 1 mm and a biaxial carbon grid on the top and bottom of the roof shell. The aim was to not only repair, but also increase the bending and normal force capacity by 50% compared to that before. The design tensile strength of the carbon textile was 1100 MPa and had a cross-section of 70.5 mm^2/m. The work on the building started in 2020 and was finished in July 2022, see Figure 2.8.

Figure 2.8: Photograph of the Hypar Shell during strengthening © Marcus Bredt (gmp Architects, n.d.)

2.4.2 TRC in Pedestrian and bicycle bridge

So far, there are a few bridges built with TRC, and they have been pedestrian and bicycle bridges. Germany is unquestionably the leading country in the production of these structures, and in 2010 the world's longest bridge made of TRC was built, see Figure 2.9 (Solidian-Kelteks, n.d.-b). The bridge, The Albstadt-Lautlingen bridge, is made of AR-glass fibres that were impregnated with epoxy resin together with fine-grained concrete with a strength class of roughly C50/60. The bridge is made up of six pre-fabricated parts that spans a total of approximately 97 m. Due to the use of TRC the minimum concrete cover used was 15 mm and the slenderness ratio ended at 1:35. The bridge is now 15 years old and there have been some challenges so far. In the concrete, slight freeze-thaw damage has appeared on the road surface as well as a few, small longitudinal cracks on the outside of the railings. However, these do not affect the load-bearing capacity of the bridge. The damaged areas, covering only approximately 2-3 square meters, resulted from challenges in the manufacturing process of the precast elements during the near-surface concrete compaction. Regular inspections and maintenance work are planned to achieve the expected service life of 80-90 years.

Figure 2.9: Photopraph of the Albstadt-Lautlingen bridge © solidian GmbH (Solidian-Kelteks, n.d.-a)

Another example is the Albstadt-Ebingen footbridge that was built in 2015 and was the first ever entirely textile carbon-reinforced concrete bridge, see Figure 2.10. The bridge was built as a pedestrian and bicycle bridge with a span of 15.55 m and a width of 3 m (Helbig et al., 2016). The sections are constructed as a trough and as a result of using textile reinforcement the walls and slab could be made thin, 70 mm and 90 mm respectively. The thin structure led to the bridge having a total

weight of 14 tons, which was approximately 50% of the weight of a RC bridge with the same span. Without the risk of corrosion that comes with conventional steel reinforcement, only a 15 mm concrete cover was needed. This kind of bridge was not yet approved in Germany at the time, and therefore an approval on individual cases (ZiE) had to be obtained by the client. This bridge showed that this kind of reinforced concrete composition could be used for large-scale applications, opening up the opportunity to use it to a greater extent in the future.

Figure 2.10: Photographs of the Albstadt-Ebingen bridge © solidian GmbH (Solidian-Kelteks, n.d.-a)

3 Tunnel linings

In addition to the previous chapter, a deeper understanding of tunnel linings was needed in order to investigate the behaviour of TRC in tunnel linings. Therefore, information about tunnel linings as well as its requirements will be presented. Furthermore, the expected behaviour of tunnel linings made with TRC will be investigated.

3.1 Concrete tunnel linings

A concrete lining is a structure that is either partly or completely a part of the load-bearing structure in a tunnel in rock. It can also be used as a cladding as a water and frost protection. The structure can be prefabricated or cast on site and can be either drained or undrained. In this report only drained tunnel linings as cladding will be investigated.

Concrete tunnel linings, especially as a main load-bearing structure, are unusual to use in Sweden, since tunnels usually are placed in rock and Sweden has favourable rock. Therefore, it is more common to use a waterproof membrane only. However, there are advantages of using concrete tunnel linings, such as that the operation and maintenance costs are small during the service life of the tunnel, if done correctly. This is because the concrete lining and the connected membrane have the same service life as the tunnel itself, meaning that it should never have to be changed during its planned service life.

Recently, a RC tunnel lining was constructed in Sweden in a rock tunnel between Dunsjö and Jakobshyttan, after investigations about its suitability. The lining was drained, cast on site and was going to work as a water and frost protection, but not be part of the load-bearing main structure. The concrete lining consisted of a concrete cladding with a waterproof membrane and a drainage mat, which are pressed against a levelling layer of sprayed concrete. The levelling layer must be smooth enough to ensure the proper installation of the membrane and drainage mat while also minimizing the accumulation of water from the surrounding rock, which could create ice lenses that damage the concrete lining. Additionally, the levelling layer serves to protect the membrane from potential punctures caused by bolts. A sketch of the section can be seen in Figure 3.1 where it is visible that the lining is cast against the contour of the tunnel with the membrane and drainage mat covering it.

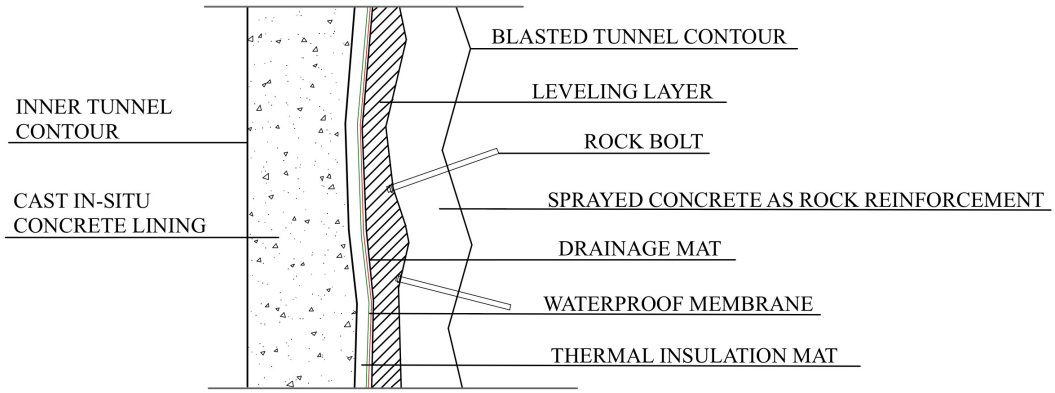

Figure 3.1: Sketch of water and frost protection with a concrete lining

3.2 Requirements

When designing tunnel linings, certain requirements must be taken into account. The requirements mentioned in this chapter are for a concrete tunnel lining used as a cladding and a drained system, and are according to Swedish transport administration.

3.2.1 Functional requirements

When the tunnel lining is used as a cladding, working as a water and frost protection that is not part of the load-bearing primary system it should have a service life of 40 years (Trafikverket, 2021). However, this is only applied when the cladding is in a space that is reachable and commutable. If the lining is cast-against the rock, the service life should instead be the same as the load-bearing primary system, whether or not it is actually a part of it. This is the case for the tunnel lining investigated in this report, resulting in the expected service life to be 120 years.

For tunnel linings the durability requirements regarding crack width and concrete cover are the same as for general concrete structures. These can be found in SS-EN 1992-2:2005 and are the same as stated in Chapter 2.3.1 Cracking and Chapter 2.3.2 Concrete cover in this report.

Another aspect to take into consideration when dimensioning a tunnel lining is the fatigue behaviour. When dimensioning the fatigue behaviour for tunnel linings with regard to air pressure and suction the requirements differ slightly depending on the planned traffic in the tunnel (Trafikverket, 2021). For car traffic the fatigue from air pressure and suction does not have to be considered. However, if the tunnel will have train traffic the number of cycles used when dimensioning should be 1×10^6.

For tunnel linings accident loads as requirements also has to be considered. These

are stated below.

Fire:
The requirements regarding fire state that the parts of the tunnel that borders a traffic space should be protected against fire according to Krav Tunnelbyggande, 7.2.2.2.1 and 8.4.4 (Trafikverket, 2021). It should be protected so that parts do not fall down or fragments being displaced and creating obstacles or hazards during escape and rescue operations. In addition, the time requirement for dimensioning is 180 minutes. According to Krav Tunnelbyggande, 6.3.2 the concrete should be prevented from spalling when the temperature is under 500°C on the concrete surface.

Explosion:
According to Krav Tunnelbyggande 8.4.5, the requirements for explosions state that a progressive landslide is not allowed to occur when a lining that is not part of the main supporting system is loaded with an explosive load (Trafikverket, 2021). However, local damage may be allowed. The lining should be dimensioned for an explosion load, see Table 3.1.

Table 3.1: Dynamic explosion load

	Compression [MPa]	**Duration [ms]**
Evenly distributed pressure in traffic space	0.1	50
Local pressure on a surface measuring 4 x 4 m in traffic space	5	2
Evenly distributed pressure in the evacuation and operation route	0.05	50

Extreme boulder load:
Extreme boulder load should be taken into consideration for non-bearing concrete linings according to Krav Tunnelbyggande 8.4.7 (Trafikverket, 2021). The load is assumed to be 60 kN acting perpendicular to the concrete lining acting on an area of 1 m x 1 m.

3.2.2 Design loads

There are also requirements on the dimensioning of different loads. For the permanent load the self-weight of the lining needed to be considered. Along with this, a tunnel lining in a rock tunnel should be dimensioned for load from falling boulder. The load should be assumed to be 6 kN acting perpendicular to the concrete lining on an area of 0,5 m x 0,5 m according to Krav Tunnelbyggande D3.2.15 (Trafikverket, 2016). For the variable load requirements some are particularly important and these are stated below.

Temperature:
According to Krav Tunnelbyggande 8.3.2.9 the dimensioning of temperature loads

for the minimum surface temperature depends on the length of the tunnel and the geographical location (Trafikverket, 2021). If the tunnel is less than or equal to 1,000 meters for train tunnels and 600 meters for traffic tunnels, it should be dimensioned for a frost index with a return period of 50 years. If the tunnel is longer, the part that is at a distance of 1000/2 or 600/2 from an end opening or cross ventilation with supply air should be dimensioned for the average frost index. The temperature data depend on the climate zone. In Krav Tunnelbyggande 8.3.2.9 (K44114) it is stated that for the maximum surface temperature in a traffic space, it should be assumed to be +20°C, regardless of the length of the tunnel and geographical location.

Air pressure and suction:
For tunnel linings where the tunnel is used for train traffic, the load from air pressure and suction from the passing trains needs to be considered. Depending on the speed of the train and the free area the air pressure and suction perpendicular to the longitudinal axis of the tunnel varies according to Krav Tunnelbyggande 8.3.2.8.2, see Table 3.2 (Trafikverket, 2021).

Table 3.2: Air pressure for one track train tunnel

Dimensioning train speed [km/h]	**Free area = 50 - 55 m^2 [kPa]**	**Free area = 53 m^2 [kPa]**
<220	± 3.0	-
250	-	± 4.5

3.3 TRC in tunnel linings

One approach to determine if TRC is a suitable material to use for tunnel linings is to compare its behaviour to the requirements for tunnel linings in general.

An issue may be the fire behaviour of TRC in tunnel linings. There have been no studies conducted investigating TRC specifically to withstand fire exposure for 180 minutes and surface temperatures of 500°C. This leads to an uncertainty regarding whether the requirements can be achieved for a tunnel lining made of TRC. As mentioned in Chapter 2.2.3 Fire resistance, mineral impregnated yarns have better fire resistance than polymer impregnated yarns, however, they have to be tested further to know their exact behaviour. Some commercially available mineral impregnated textile meshes has been developed more recently, however they are limited and there are no standardizations of them as for epoxy impregnated meshes. If no TRC systems are able to meet these requirements, alternative solutions such as a fire resistance board or a thicker concrete cover could be an alternative.

As mentioned in Chapter 2.2.3 Fire resistance, the risk of spalling is also a factor that needs to be considered when discussing fire behaviour. However, the risk of spalling is not the most critical factor, when comparing to the loss of bond strength.

As for the remaining requirements, TRC reaches them according to the research and studies that has been covered in this report. In summary, TRC should be an appropriate material to use in tunnel linings, however further research should definitely be considered in order to fully utilize the beneficial factors of TRC.

4 FE-model

For the case study, a tunnel lining was investigated with the purpose of designing one tunnel lining using RC and one using TRC. The following chapter presents the inputs for the model as well as the results from the analyses.

4.1 Limitations for case study

The loads considered in the case study are based on the requirements of tunnel linings, see Chapter 3.2 Requirements. However, for the modelling only the design loads, see Chapter 3.2.2 Design loads, were considered. The functional requirements: extreme boulder load, explosion, fatigue, see Chapter 3.2.1 Functional requirements, are not taken into account for the modelled tunnel lining.

4.2 Geometry

For the model, a tunnel lining was conducted based on measurements of a typical cross-section of a two-track train tunnel from the Swedish transport administration. The lining was modelled as a polycurve in Grasshopper consisting of straight lines and curves with 2 different radii, see Figure 4.1. The polycurve was then divided into a number of beam elements in order to model the lining as a beam in FEM-design. The number of elements was determined through a convergence study see Chapter 4.7.2 Convergence study.

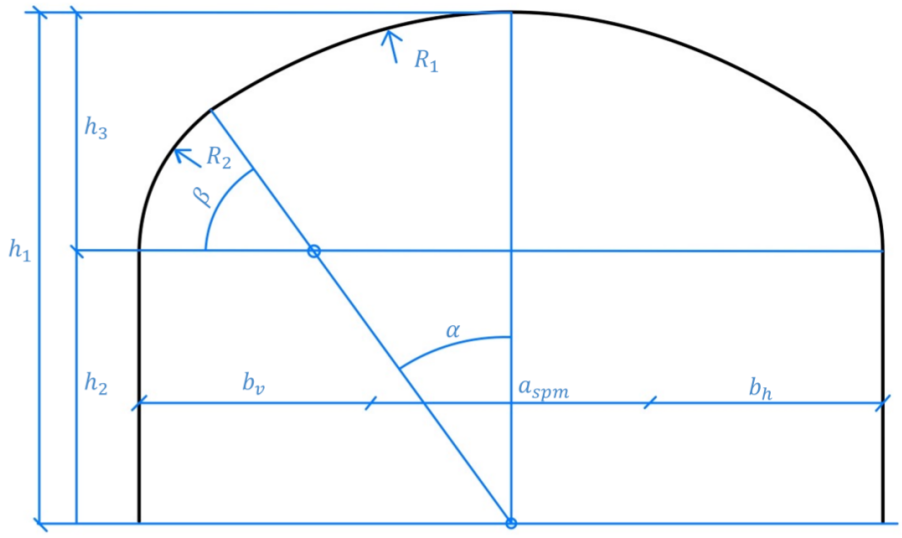

Figure 4.1: Section of two-track train tunnel

The measurements used for the tunnel lining design were taken from the Swedish transport administration, see Table 4.1.

Table 4.1: Measurements for two-track train tunnel

Label	Measurements
b_v	3.75 m
b_h	3.75 m
a_{spm}	4.5 m
h_1	8.25 m
h_2	4.4 m
h_3	3.85 m
R_1	8.25 m
R_2	2.8 m
α	36 °
β	54 °

The tunnel lining was modelled according to the dimensions above, with the beam elements having a width of 1 meter. The thickness of the tunnel lining varied during the optimization process.

4.3 Material Parameters

For concrete tunnel linings, concrete C35/45 is usually used and therefore its material parameters were chosen for the tunnel lining made of RC. For the steel reinforcement, the material parameters of B500B were used.

For the tunnel lining made of TRC, the material parameters of concrete C50/60 were used, since it corresponds to high-strength fine-grained concrete which is typically used for TRC, as mentioned in Chapter Concrete 2.1.1. For the tunnel lining with TRC, the material parameters of a commercially available textile mesh from Solidian Kelteks were used (solidian GmbH, 2024),see Figure 4.2. The density of concrete was set to 2550 kg/m^3 as a default in FEM-design for all concrete classes.

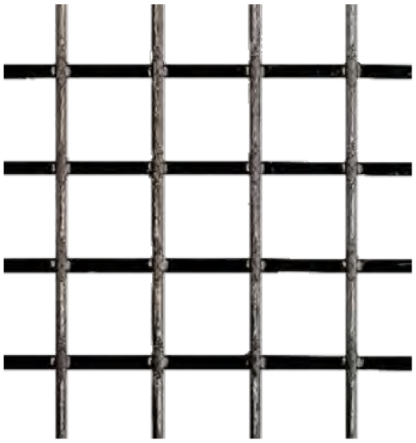

Figure 4.2: Structure of textile mesh Solidian GRID Q95-CCE-38

The geometry parameters of the textile mesh can be seen in Table 4.2 and its mechanical properties are stated in Table 2.2 in Chapter 2.2.5 Mechanical properties.

Table 4.2: Geometry and structure parameters for textile mesh Solidian GRID Q95-CCE-38

Parameter		**Value**
Nominal cross-sectional area per fibre strand	A_{nm}	8.8 mm^2
Nominal cross-sectional area per meter per fiber strand	a_{nm}	232 mm^2
Grid width	S	38 mm
Grid height	h_g	3.3 mm

4.4 Boundary conditions

In reality the bottom supports of a tunnel lining can vary and be complex depending on the material of the foundation on which the tunnel is constructed. For the purpose of this case study, a simplification was made by using hinged bottom supports in the modelled tunnel lining. The interaction between the rock bedding and the lining was modelled using springs acting only in compression. The springs had a linear stiffness of 200 MN/m^3 in compression and zero stiffness in tension. The parameters were chosen based on a previous study, see Figure 4.3 (Berrocal et al., 2018).

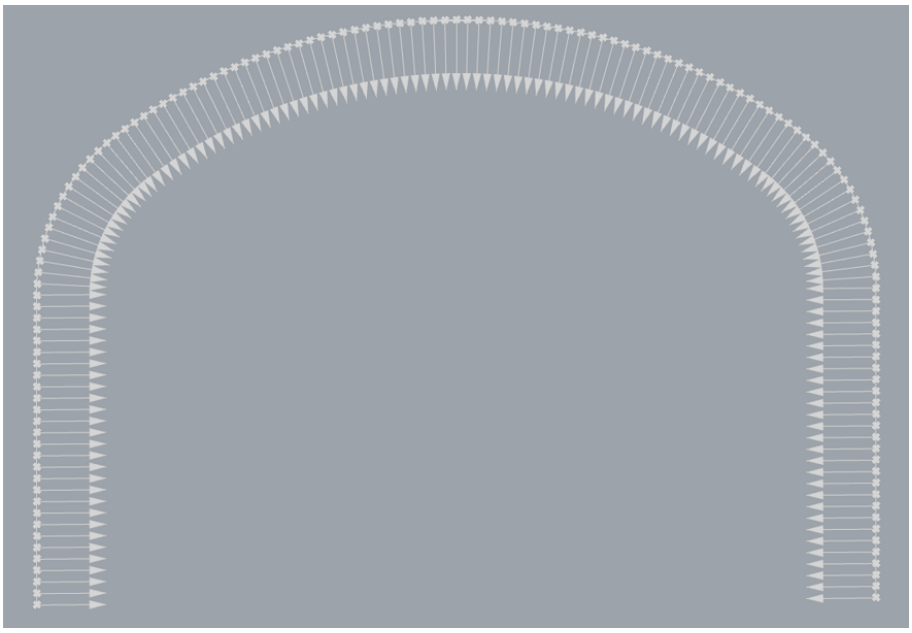

Figure 4.3: Visualization of direction of springs

4.5 Loads

All loads that were used in the model were according to the design loads mentioned in Chapter 3.2.2 Design loads. The self-weight of the lining was placed as a line

load along the whole length of the curve. The other permanent load was the boulder load, which was modelled as a line load of 3 kN/m on a line of 0.5 m. To determine the most critical position of the boulder load, a moving load was used in FEM-design. By changing the position of the load and analysing the deflection, it could be observed that the middle of the arc was the most unfavourable position for the load placement. Therefore, the boulder load was placed there for the analyses.

Further on, two loads were conducted considering the temperature variation through the lining. Two scenarios were established: one for the maximum surface temperature, and one for the minimum surface temperature, according to Chapter 3.2.2 Design loads "Temperature". For the minimum surface temperature, the value considering the temperature of the rock was set to 8°C and the bottom value representing the lowest allowed temperature in the tunnel was set to -15°C, which represent climate zone 1 in Sweden. For the maximum surface temperature, the value considering the temperature of the rock was still 8°C and the top value representing the highest allowed temperature in the tunnel was set to +20°C.

The final variable load that was modelled was the air pressure/air suction. The load was dimensioned as 3 kPa acting along the entire length of the lining. This value is for trains that have a speed below 220 km/h, and chosen because this is the maximum speed for trains in Sweden (Trafikverket, 2020). It was modelled as a line load acting on the inside, pushing out, or on the outside, pushing in depending on the load being modelled as pressure or suction.

4.6 Load combinations

In order to determine the most critical case for the loads, different load combinations were constructed. For the load combinations, Equations 6.10a and 6.10b from SS-EN-1990, chapter 6, was used (SS-EN-1990, 2014). Below the load combinations are stated and named depending on whether 6.10a or 6.10b was used.

The initial load combination consisted of the permanent loads: the self-weight and boulder load, see Equation 4.1. This was to get an estimate on the behaviour of the structure when only permanent loads were acting on the model.

Self-weight and boulder load:

$$LC_1 = 1.35 \cdot (G_k + q_{k.boulder}) \tag{4.1}$$

In addition, a load combination consisting of the permanent loads along with the air pressure load and the air suction load was constructed, respectively. Four load combinations were done, two for air pressure using 6.10a and 6.10b, see Equation 4.2 and Equation 4.3, and two for air suction using the same two equations, see Equation 4.4 and Equation 4.5. The value of $\psi_{0.suction}$=$\psi_{0.pressure}$=0.8 comes from SS-EN-1990,

Table A2.3.

Self-weight, boulder load and air pressure:

$$LC_{2a} = 1.35 \cdot (G_k + q_{k.boulder}) + q_{k.pressure} \cdot \psi_{0.pressure} \tag{4.2}$$

$$LC_{2b} = 1.15 \cdot (G_k + q_{k.boulder}) + q_{k.pressure} \tag{4.3}$$

Self-weight, boulder load and air suction:

$$LC_{3a} = 1.35 \cdot (G_k + q_{k.boulder}) + q_{k.suction} \cdot \psi_{0.suction} \tag{4.4}$$

$$LC_{3b} = 1.15 \cdot (G_k + q_{k.boulder}) + q_{k.suction} \tag{4.5}$$

It was noted that the load combination with air suction was the most critical between the air pressure and the air suction load, and therefore only the air suction load was used in further load combinations.

For the load combination containing the two temperature loads, two of each load had to be constructed, one for the "negative" and one for the "positive" temperature load, see Chapter 4.6 Load combinations "Temperature".

Therefore, six load combinations were constructed for all dimensioned loads. Two using 6.10a where no variable load is considered main load, see Equation 4.6 and Equation 4.7. The value of $\psi_{0.temp}$=0.6 comes from SS-EN-1990, Table A1.1.

Self-weight, boulder load, air suction and temperature variation:

$$LC_{4a.temp.neg} = 1.35 \cdot (G_k + q_{k.boulder}) + 1.5 \cdot q_{k.temp.neg} \cdot \psi_{0.temp} + 1.5 \cdot q_{k.suction} \cdot \psi_{0.suction} \tag{4.6}$$

$$LC_{4a.temp.pos} = 1.35 \cdot (G_k + q_{k.boulder}) + 1.5 \cdot q_{k.temp.pos} \cdot \psi_{0.temp} + 1.5 \cdot q_{k.suction} \cdot \psi_{0.suction} \tag{4.7}$$

The other four equations were formulated using 6.10b , with the temperature load and the suction load applied as the main load respectively, see Equation 4.8, Equation 4.9, Equation 4.10 and Equation 4.11.

Temperature as main load:

$$LC_{4b.temp.neg} = 1.15 \cdot (G_k + q_{k.boulder}) + 1.5 \cdot q_{k.temp.neg} + 1.5 \cdot q_{k.suction} \cdot \psi_{0.suction} \tag{4.8}$$

$$LC_{4b.temp.pos} = 1.15 \cdot (G_k + q_{k.boulder}) + 1.5 \cdot q_{k.temp.pos} + 1.5 \cdot q_{k.suction} \cdot \psi_{0.suction} \tag{4.9}$$

Air suction as main load:

$$LC_{4b.suction.temp.neg} = 1.15 \cdot (G_k + q_{k.boulder}) + 1.5 \cdot q_{k.temp.neg} \cdot \psi_{0.temp} + 1.5 \cdot q_{k.suction} \quad (4.10)$$

$$LC_{4b.suction.temp.pos} = 1.15 \cdot (G_k + q_{k.boulder}) + 1.5 \cdot q_{k.temp.pos} \cdot \psi_{0.temp} + 1.5 \cdot q_{k.suction} \quad (4.11)$$

For the chosen design, the crack width limitation for RC was also checked, which was done by SLS load combinations using simplified calculations. These are presented in Chapter 5.1.1 Check of crack width.

4.7 Verification

In order to verify the model to ensure that all components, including boundary conditions and loads, were modelled accurately, analytical calculations were done. In addition to this, a convergence study was conducted in order to obtain the optimal number of elements for the modelled concrete lining.

4.7.1 Analytical calculations

The analytical calculations consisted of the reaction forces when only considering the self-weight of the tunnel. The analytical calculations done for the reaction force in the left hinged support resulted in 82.53 kN and the reaction force from the model for the same support resulted in 82.58 kN. This gave a difference of 0.05 kN which was considered acceptable. The full calculations can be seen in Appendix A.

4.7.2 Convergence study

For the convergence study, the self-weight was applied to analyse the behaviour of the maximum deflection of the tunnel lining, in relation to number of beam elements. The convergence study can be seen in Figure 4.4.

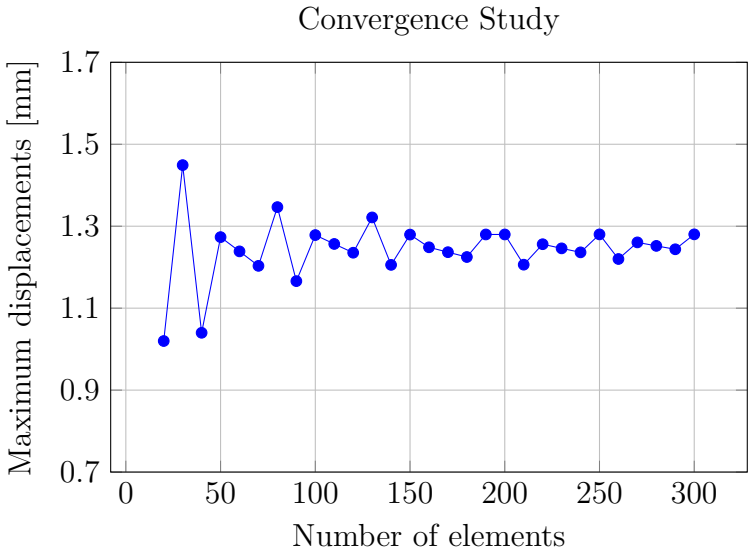

Figure 4.4: Convergence study for tunnel lining

A possible reason for the large fluctuation in the graph could be because of the stiffness in the springs only being applied in one direction, in this case only in compression. This leads to a non-linear behaviour of the springs. In order to ensure this, a convergence study of the structure modelled with springs acting in both compression and tension was performed, as well as a convergence study modelled without any springs was done, see Figure B.1 and Figure B.2 in Appendix B. This showed that the springs had a non-linear behaviour.

As seen in Figure 4.4 the graph converges when increasing the number of elements, and it can be established that around 150 elements are needed to perform an accurate analysis. The high number of elements to reach convergence is due to the non-linear behaviour of the springs.

4.8 FE results

From FEM-design, the maximum moment and normal force were extracted for the most critical section for all load combinations for the design in ULS, mentioned in Chapter 4.6 Load combinations. For different thicknesses, the most critical section and the most critical load combination varied. The results are presented in Table 4.3 where the positive moment is oriented inward, into the tunnel.

Table 4.3: Maximum moment and normal force for different cross-section thicknesses

Thickness of lining [mm]	**Moment C35/45 [kNm]**	**Normal force C35/45 [kN]**	**Moment C50/60 [kNm]**	**Normal force C50/60 [kN]**
60	-23.25	-38.60	-23.25	-38.60
70	-25.55	-40.90	-25.55	-40.90
80	-27.85	-43.10	-27.85	-43.10
90	-30.16	-45.40	-30.16	-45.40
100	-32.50	-48.30	-32.50	-48.30
110	-34.87	-50.60	35.00	-30.90
120	-37.23	-53.00	38.56	-31.80
130	40.81	-32.77	42.30	-32.80
140	44.51	-33.72	45.98	-33.90
150	48.38	-34.69	50.10	-34.90

As seen in Table 4.3, the maximum moment and normal force were the same for concrete C35/45 and C50/60 for thicknesses 60 mm to 100 mm. When the thickness was 110 mm or larger the results between the two materials differs. Furthermore, the most critical section when using concrete C35/45 appeared in the "corner" of the tunnel lining for the smaller thicknesses up to 130 mm, hence the results being negative. In contrast, when using concrete C50/60 the most critical section was in the "corner" for the smaller thicknesses as well, but only up to thickness 110 mm instead. The reason why this change occurs at different thicknesses for the two concrete classes was due to the different stiffnesses of the materials. Since the structure was statically indeterminate, the stiffness significantly influenced the moment distribution.

The load combination that was the most critical for the thinner thicknesses, when the moment was negative, was Equation 4.4, seen in Chapter 4.6 Load combinations. For all thicknesses with a negative maximum moment the distribution was similar, an example of this kind of moment distribution can be seen in Figure 4.5.

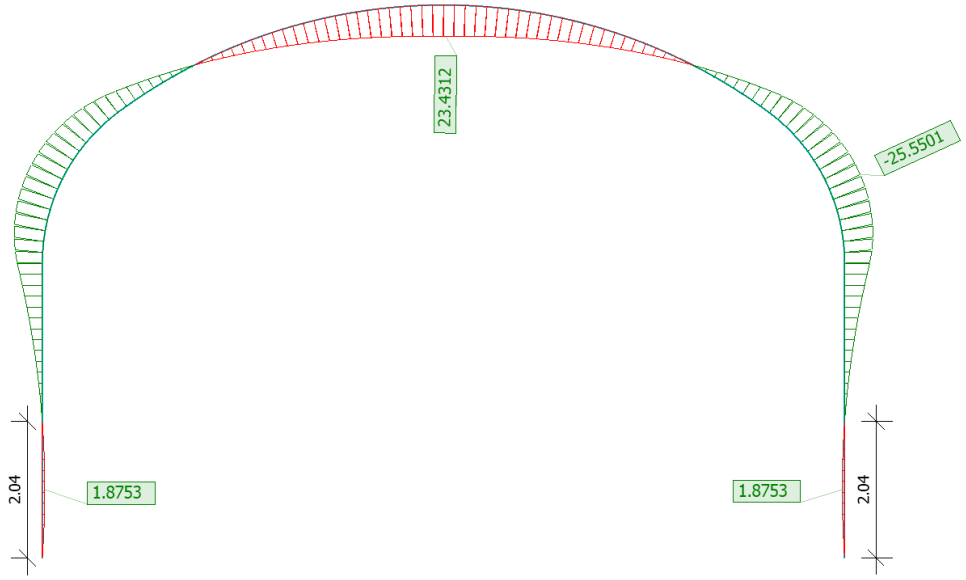

Figure 4.5: Moment distribution of tunnel lining with 70 mm thickness

For thicker thicknesses, where the maximum moment was positive, the most critical section was in the middle of the tunnel. The load combination that was the most critical for the thicker thicknesses was Equation 4.8 seen in Chapter 4.6 Load combinations. For all thicknesses with a positive maximum moment the distribution was similar, an example of this kind of moment distribution can be seen in Figure 4.6.

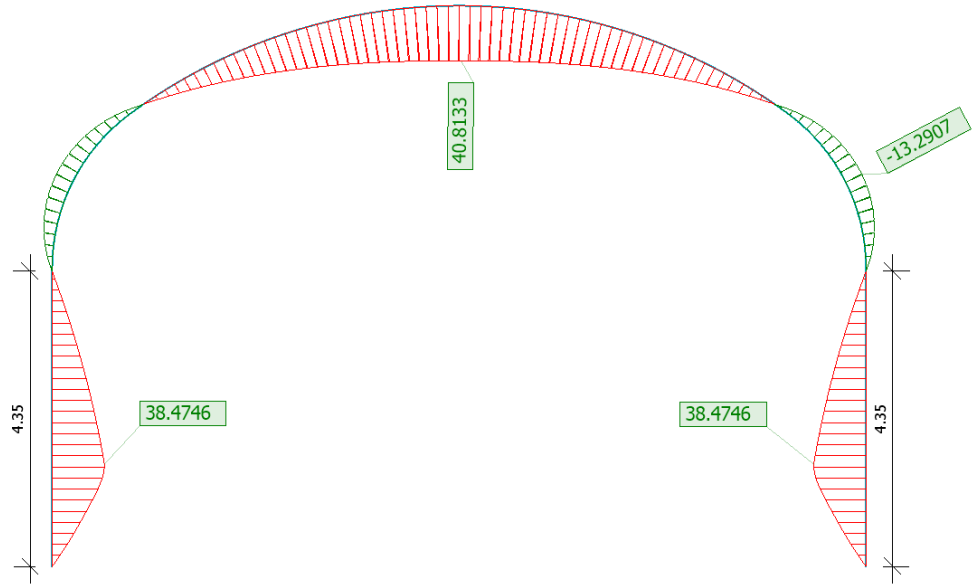

Figure 4.6: Moment distribution of tunnel lining with 130 mm thickness

The variation in which load combinations produced the most critical section was primarily due to the thickness of the tunnel lining. This also explains the differences

in moment distribution. For thinner linings, the effect of self-weight was relatively small compared to other loads, whereas for thicker linings, the influence of self-weight became more significant and caused the surrounding springs to engage more, which resulted in greater inward pressure. The maximum positive and negative moment, normal force for the maximum moment as well as the maximum shear force in the tunnel lining, for every load combination, for thickness 70 mm and 130 mm, are presented in Appendix F.

5 Design of tunnel lining

The designs of the tunnel linings for RC and TRC were done using the maximum moment and normal force, as well as the shear force, extracted from the analysis done in FEM-design 24. All calculations for the designs of tunnel linings can be seen in Appendix C and Appendix D, and calculations for the CO_2-eq emissions can be seen in Appendix E.

5.1 Design of RC tunnel lining

The design of the tunnel lining made of RC was an iterative process. The design was optimized so that the total CO_2-eq emissions for the tunnel lining were minimized. The design of the cross-section was per meter width of the lining, while the height of the cross-section, along with the steel bar diameter and amount of bars was decided through an iterative process. Initially, the optimized amount of bars and their diameter were calculated for different heights. The amount of material needed for each height was then used to calculate the total CO_2-eq emissions in order to determine which height of cross-section gave the lowest emissions, see Table 5.1. A visualisation of these results can be seen in Figure 5.1.

For the CO_2-eq calculations the values of the CO_2-emissions for each material comes from production. Concrete C35/45 was used for the RC tunnel lining where a value of 286 kg CO_2-eq/m^3 was used (Concrete Sustainability Council, 2022). For the steel, a value of 2.3 kg CO_2-eq/kg was used (Friese et al., 2022). For further calculations, see Appendix E.

Table 5.1: Amount of reinforcement and CO_2-eq emissions of different heights of RC cross-section

Height of cross-section [mm]	**Bars in bottom layer**	**Bars in top layer**	**CO_2-eq emissions [kg]**
150	7ϕ16 mm	4ϕ'8 mm	1623
140	7ϕ16 mm	4ϕ'8 mm	1553
130	7ϕ16 mm	3ϕ'8 mm	1456

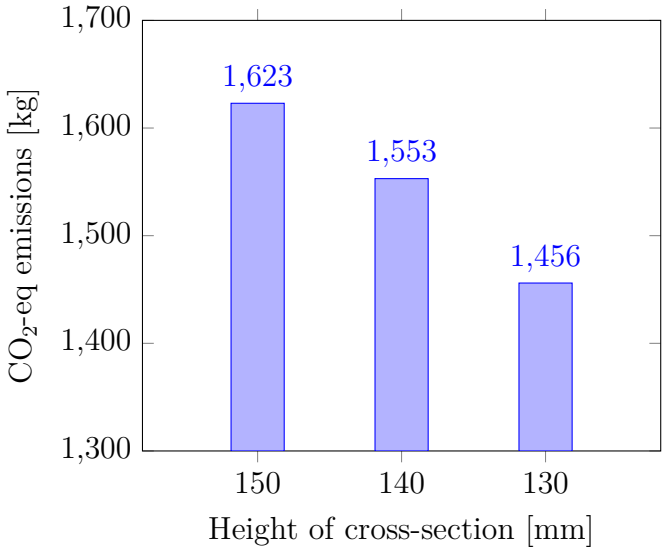

Figure 5.1: CO_2-eq emissions for different heights of RC cross-section

The lowest achievable height of the cross-section was 130 mm since a lower height would result in an insufficient concrete cover, meaning that the required number of bars would not fit. The necessary concrete cover thickness was calculated and resulted in 35 mm. The result was also verified by confirming that the design moment (M_{Ed}) was smaller than the moment capacity of the designed cross-section (M_{Rd}). The utilization ratio between M_{Ed} and M_{Rd} resulted in 89.3%. The shear capacity was also checked and verified for the cross-section. For further calculations, see Appendix C.

The amount of reinforcement needed varied over the length of the tunnel lining depending on the moment distribution and the positions of zero moment, see Figure 4.6 in Chapter 4.8 FE results. For the walls and the arch, the needed bottom reinforcement was 7 bars with the diameter of 16 mm and the needed top reinforcement was 3 bars with the diameter of 8 mm, according to the requirement of minimum reinforcement. This cross-section is shown in Figure 5.2.

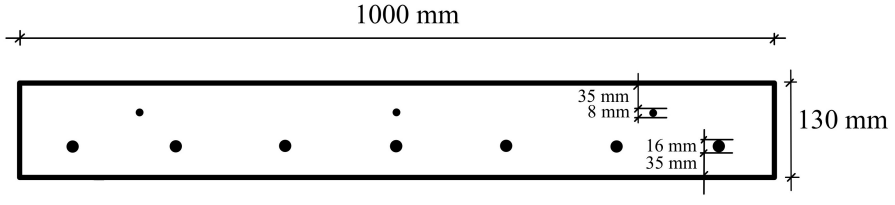

Figure 5.2: Cross-section for RC in most critical section

For the "corners" of the lining no reinforcement was needed with regard to cracking, however, according to the same requirement as previously mentioned, three bars of 8 mm diameter was placed as the top and bottom reinforcement. This cross-section can be seen in Figure 5.3.

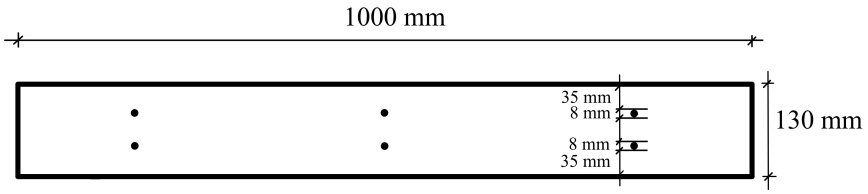

Figure 5.3: Cross-section for RC in "corners"

The distribution of the reinforcement for the entire tunnel lining is shown in Figure 5.4.

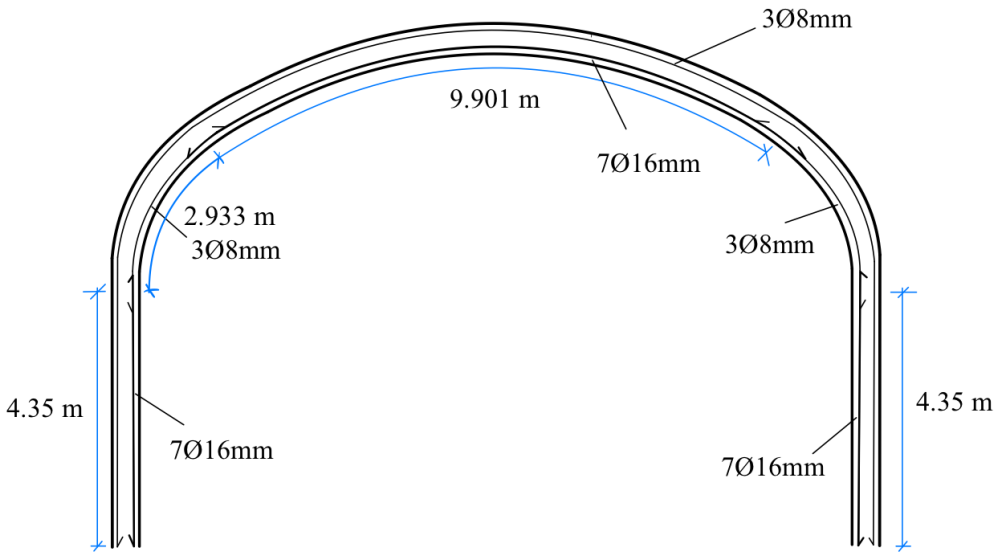

Figure 5.4: Reinforcement distribution in RC tunnel lining

5.1.1 Check of crack width

For the tunnel lining in RC, the crack spacing and crack width were calculated for quasi-permanent load combinations (SLS) using SS-EN-1992-1-1:2005, see Equation 5.1.

$$LC_{quasi-permaent} = (G_k + q_{k.boulder}) + \sum \psi_{2.i} \cdot q_{k.i} \tag{5.1}$$

The quasi-permanent load combinations meant only the permanent loads were applied since $\psi_{2.i} = 0$ for all variable loads, and it resulted in a crack width of 0 mm. This meant that the crack width was not dimensioning for this cross-section.

The effect on the crack width from shrinkage over time was also considered. Since the analysis software cannot model non-uniform shrinkage directly, this was instead approximated by applying a negative temperature load. To simulate the non-linear shrinkage loads in SLS, the calculation of crack width was performed using the

negative temperature load applied in ULS, but as a permanent load instead, see Equation 5.2.

$$LC_{quasi-permaent} = (G_k + q_{k.boulder} + q_{k.temp.neg}) + \sum \psi_{2.i} \cdot q_{k.i} \tag{5.2}$$

This gave a simplified model of the shrinkage over time and resulted in a crack width of 0.164 mm, which is within the requirement of crack width for concrete structures, see Chapter 2.3.1 Cracking. Calculations of the crack width can be seen in Appendix C.

5.2 Design of TRC tunnel lining

The design of the tunnel lining made of TRC presented certain challenges due to the absence of established design standards specific for TRC. While the general calculation principles remained comparable to those used for RC, there is currently no standardized methodology for designing TRC cross-sections. The design in ULS was carried out and is presented below. However, crack width calculations were not performed due to the lack of applicable design standards for TRC.

Since there is no Swedish design standard for TRC yet and the chosen textile mesh is produced in Germany, the German design standard was used for this case. According to the German design standard, a partial safety factor for the textile reinforcement of $\gamma_{nm} = 1.3$ was applied. Additionally, for the selected mesh type (Solidian keltech Q95-CCE-38), an efficiency factor of $\eta_f = 0.83$ was used, according to T.Knobloch at Solidian GmbH (personal communication, May 8th, 2025). This efficiency factor is specific for the chosen mesh and is used since the textile mesh cannot utilize its full tensile strength and therefore needs to be reduced.

The mesh had predetermined yarn dimensions and fixed spacing between the yarns (grid width). Therefore, the only variables that could be adjusted during the optimization process, were the height of the cross-section and the number of reinforcement layers. The resulting CO_2-eq emission for each tested height can be seen in Table 5.2 as well as visualized in Figure 5.5. In the table the trend points at that thicker cross-sections than 100 mm were not optimal.

For the CO_2-eq calculations the values of the CO_2-emissions for each component of the material comes from production. For TRC concrete C50/60 was used and therefore a value of 325 kg CO_2-eq/m^3 was used (Concrete Sustainability Council, 2022). For the carbon fibres a value of 19.7 kg CO_2-eq/kg was used (Friese et al., 2022). For further calculations, see Appendix E.

Table 5.2: Needed number of textile mesh and CO_2-eq emissions of different cross-section TRC

Height of cross-section [mm]	**Number of textile layers**	**CO_2-eq emissions [kg]**
100	3	1231
90	3	1151
80	3	1071
70	3	992

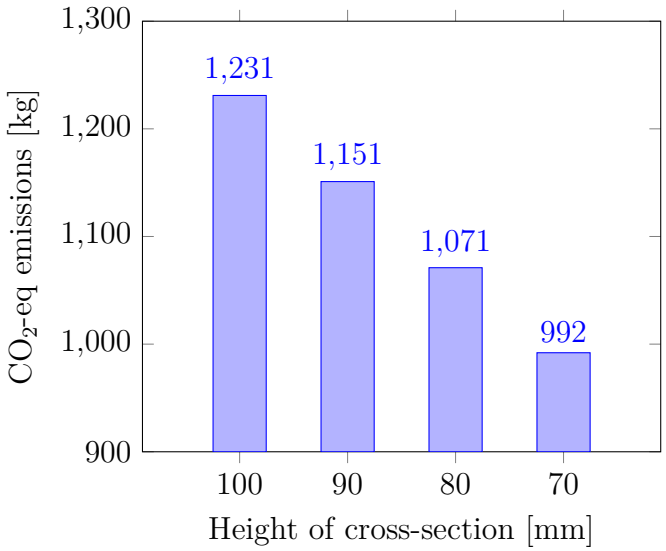

Figure 5.5: CO_2-eq emissions for different heights of TRC cross-section

Using this design method as well as the textile mesh mentioned, the lowest possible height of the cross-section resulted in 70 mm with 3 layer mesh, otherwise the textile layers needed did not fit within the cross-section. A concrete cover of 10 mm was used according to Chapter 2.3.2 Concrete cover. The grain size in the concrete was set to 6 mm, according to Chapter 2.1.1 Concrete, and therefore the distance between the layers of mesh was set to 8 mm. The utilization ratio between the design moment (M_{Ed}) and moment capacity (M_{Rd}) resulted in 79.3%. The shear capacity was also checked for the cross-section. For further calculations, see Appendix D.

The needed number of textile reinforcement layers was 3 for almost the entire tunnel lining, and the design of the cross-section is shown in Figure 5.6. A detailed sketch of the placement of textile reinforcement layers can be seen in Figure 5.7

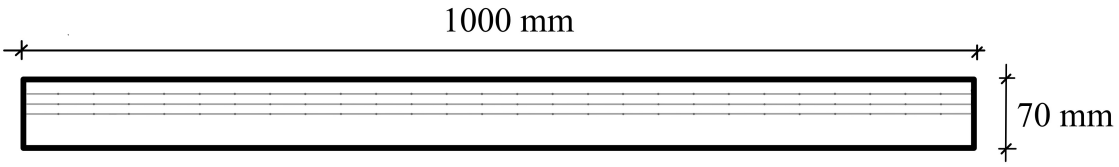

Figure 5.6: Cross-section for TRC in most critical section

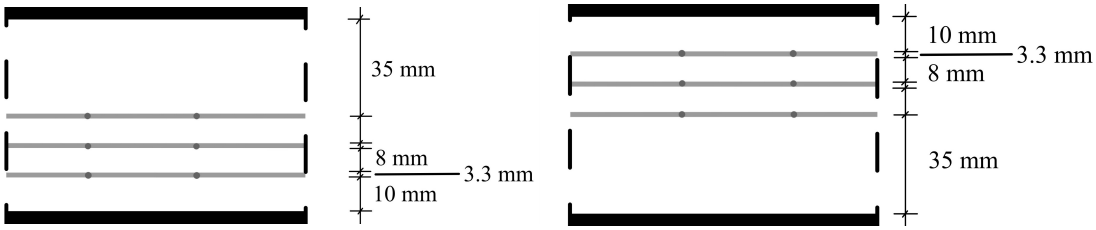

Figure 5.7: TRC reinforcement in top and bottom

The layers were distributed according to the moment distribution, see Figure 4.5 in Chapter 4.8 FE results. For the lowest part of the wall no reinforcement was needed with regard of cracking, however one of the layers was continued along the whole length of the wall. There are no set requirements in Sweden for minimum reinforcement when using TRC, therefore, this was only an assumption made. The same layer ran continuously along the whole length of the tunnel lining. The distribution of the layers over the tunnel lining can be seen in Figure 5.8.

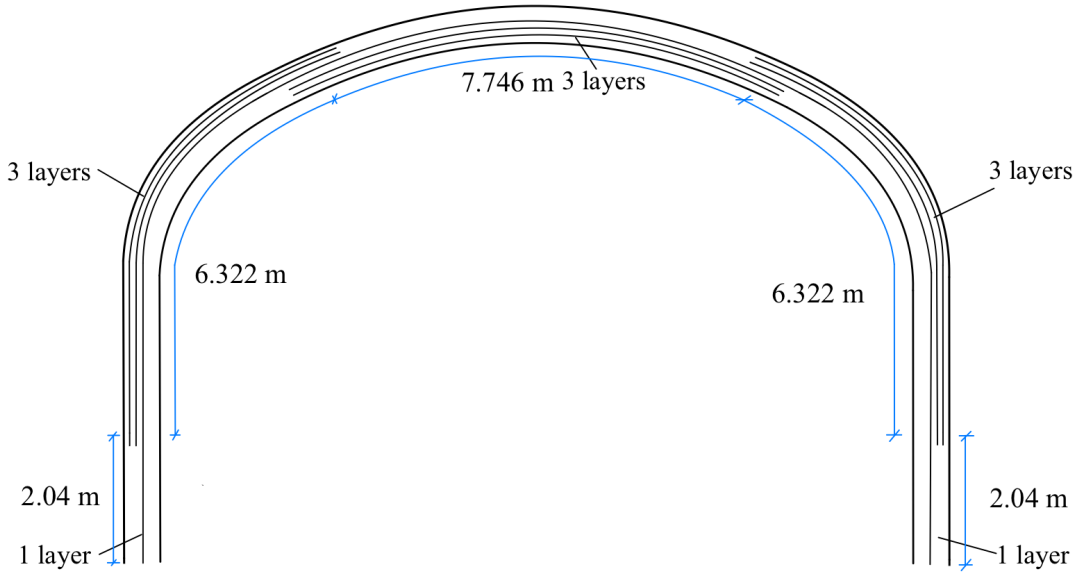

Figure 5.8: Reinforcement distribution in TRC tunnel lining

5.3 Comparison of the designed tunnel linings

A comparison of the two designs is presented in Table 5.3. The cross-section using TRC resulted in a reduction of 46% in the height of the cross-section and 46% in the amount of concrete needed for the whole tunnel lining. The reduction of concrete is mainly due to the possibility of reducing the concrete cover when using TRC. It also showed a reduction of 45% in the amount of reinforcement needed when using textile reinforcement instead of steel reinforcement. Further on, it also showed a reduction of 464 kg or 32% of CO_2-eq emissions for the tunnel lining.

Table 5.3: Comparison of the designed RC and TRC tunnel linings

	RC	**TRC**	**Reduction**
Height of cross-section [mm]	130	70	46%
Amount of concrete [m^3]	3.1	1.7	46%
Amount of reinforcement [m^3]	0.031	0.017	45%
Net CO_2-eq emissions [kg]	1 456	992	32%
Utilization ratio [%]	89.3	79.3	-

The bar diagram below, see Figure 5.9, shows the distribution of CO_2-eq emissions for the designed tunnel linings using RC and TRC. For RC, the concrete took up a majority of the emissions and for TRC it took up around half of the total emissions. A noticeable part of the diagram is that the emissions of the concrete and reinforcement used in TRC were smaller than both of its corresponding materials used in RC. As expected, the largest difference was between the CO_2-eq emissions from the concrete used in the two tunnel linings, which shows how large the impact of the amount of concrete used is on the net CO_2-eq emissions.

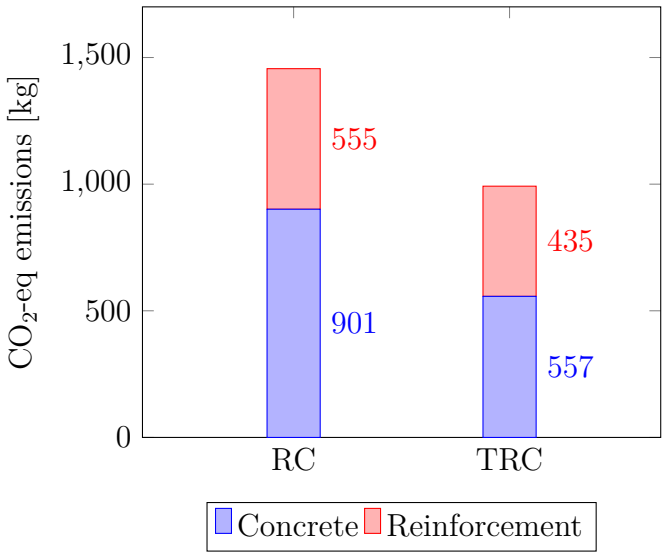

Figure 5.9: CO_2-eq emissions for the different components of RC and TRC

6 Discussion

As presented in Chapter 5.3 Comparison of the designed tunnel linings, there was a significant difference in the emissions of CO_2-eq. This is mainly due to the large reduction of concrete in the TRC cross-section. Although the carbon mesh has larger CO_2-eq emissions per kg than the steel, the emissions are clearly lower for the carbon mesh due to its light weight. Therefore, it is the amount of concrete used that will be the determining factor for the CO_2-eq emissions of a cross-section.

A lower height of the TRC cross-section may be achievable through further design optimizations. One potential approach is to reduce the thickness of the concrete cover. Since textile reinforcement is not yet governed by standardized design codes, it may be reasonable to assume that the required concrete cover could be even thinner than 10 mm, taken from EN1992-1-1:2023, regarding FRP. However, a thicker concrete cover contributes to improved fire resistance. Therefore, depending on the fire resistance properties of the textile mesh used, a thinner or thicker concrete cover may be required. Additionally, in the current design, a spacing of 8 mm between reinforcement layers was used. This spacing could potentially be decreased, allowing for additional layers to be accommodated within the same cross-sectional height.

Another approach to reducing the height of the TRC cross-section is to optimize the textile mesh itself. As described in Chapter 5.2 Design of TRC tunnel lining a commercially available textile mesh was used with its specific design parameters. It is crucial to have known parameters of the reinforcement for the calculations, and therefore, no modifications were made to the textile mesh. However, by altering the mesh design, specifically by reducing the spacing between yarns, it would be possible to incorporate more yarns per meter. This increase of yarns could potentially enhance the tensile strength of the composite. As a result, fewer layers of mesh may be required and a lower cross-sectional height could be possible. However, if modifications are made to the mesh, it would be essential to experimentally determine the new design parameters to ensure an accurate and reliable structural design based on the modified mesh properties.

One could argue that, given the 38 mm grid size of the selected mesh and grain size of 6 mm in the concrete, reducing the spacing between the yarns would not inflict on the concrete's ability to penetrate the reinforcement. However, a smaller spacing could cause other issues, such as the concrete cover detaching from the rest of the structure under bending loads. This is a factor that the manufacturer of the mesh may already have considered, and the current mesh configuration may therefore represent an optimized design. Consequently, increasing the number of yarns per meter might not be possible.

Further optimization of the tunnel lining designs could be achieved by varying the thickness along its length. The bending moment in the structure varies with the length of the tunnel lining, being significantly smaller in certain parts compared to

the maximum moment. This results in the cross-section being over dimensioned in certain areas of the structure. A possible way to optimize the structure is, therefore, to modify the thickness of the tunnel lining according to the varying moment. This modification could be done for both cross-sections in order to reduce the concrete used. However, varying the thickness along the length of the tunnel lining may become an issue during production. If the variation in cross-section height is within small tolerances, it can complicate in situ construction. This aspect could be further investigated in order to determine the possibility of the production of a tunnel lining with a varying cross-section height.

7 Conclusion

This thesis has examined the feasibility and potential benefits of using textile reinforced concrete (TRC) as an alternative to conventional steel reinforced concrete (RC) in tunnel linings. Through a combination of a literature study and a case study, the structural behaviour and environmental impact of TRC were critically assessed.

The findings indicate that TRC presents significant advantages over RC in certain contexts. Its corrosion-resistant properties eliminate the need for a thick concrete cover, allowing for more slender and lightweight structures. The case study showed that the possibility to reduce the concrete cover, when using TRC, strongly influenced the total CO_2-eq emissions compared to RC, which highlights the environmental benefits of TRC.

The literature study showed that structurally, TRC demonstrated sufficient load-bearing capacity and good fatigue behaviour under cyclic loading, which is crucial for tunnels subjected to air pressure and air suction from train traffic. However, concerns remain regarding its fire performance, particularly the deterioration of polymer impregnated meshes at elevated temperatures. Mineral impregnated alternatives offer some promise but require further testing and standardization.

The numerical modelling confirmed that TRC can meet structural requirements under relevant load cases. The optimized TRC cross-section was thinner and lighter than the RC equivalent, while still fulfilling critical requirements set for tunnel linings. However, since there are no current design standards for TRC in Sweden, further development is necessary.

Overall, the study concludes that TRC is a promising alternative to RC in tunnel lining applications, especially from a sustainability and material efficiency perspective.

7.1 Suggestions for further research

The literature study highlighted the need for further research of the fire resistance of the impregnations of the textile meshes used in TRC. The behaviour of the bond between the mesh and concrete at elevated temperature needs to be investigated through experimental testing.

As stated in the limitations of this report, no calculations were performed for shrinkage or creep. Moreover, the serviceability limit state (SLS) was only addressed to a limited extent. Several of the specified functional requirements, such as extreme boulder load, explosion load and fatigue were not considered in the case study. These aspects require further investigation before the material can be considered for

practical structural applications.

The environmental impact of the designs done in this report was simplified and could therefore be further investigated. In particular, the emissions resulting from material transportation should be investigated, as the weight differences between the materials are considerable.

Further research should also examine the economic implications of replacing conventional reinforced concrete (RC) with textile reinforced concrete (TRC), as this aspect has not been addressed in the present study. The economic viability of TRC depends on several factors. In particular, the introduction of a new construction material can involve higher initial costs due to limited standardization, low production volumes, and uncertain market demand.

References

Ahsan, R. (n.d.). *Fatigue in Concrete Structures* (tech. rep.).

Berrocal, C. G., Löfgren, I., & Lundgren, K. (2018). *Assessment of cast-in-situ FRC linings for high-speed railway tunnels with respect to fatigue and cracking* (tech. rep.).

Blomqvist, I. (2021). *Textile Reinforced Concrete Structures - Bending tests of one-way slabs* (tech. rep.).

Brameshuber, W., & Brockmann, T. (2006). *Textile Reinforced Concrete, State-of-the-Art* (tech. rep.). RILEM Technical Committe. Bagneux, France, RILEM Publication.

Brockmann, T. (2007). Mechanical and Fracture Mechanical Properties of Fine Grained Concrete for TRC Structures. In C. U. Grosse (Ed.), *Advances in construction materials 2007* (pp. 119–129). Springer Berlin Heidelberg. https://doi.org/10.1007/978-3-540-72448-3{_}12

Chahar, A. S., & Pal, P. (2022). Study on various properties of reinforced concrete – A review. *Materials Today: Proceedings*, *65*, 597–602. https://doi.org/10.1016/J.MATPR.2022.03.193

Concrete Sustainability Council. (2022). *Concrete Sustainability Council CO2-Module: Annex* (tech. rep.). https://www.concretesustainabilitycouncil.com/

Friese, D., Scheurer, M., Hahn, L., Gries, T., & Cherif, C. (2022). Textile reinforcement structures for concrete construction applications—a review. *Journal of Composite Materials*, *56*(26), 4041–4064. https://doi.org/10.1177/00219983221127181

Fürst, R., Hejtmánek, P., Vlach, T., Řepka, J., Mózer, V., & Hájek, P. (2022). Experimental Evaluation of Carbon Reinforced TRC with Cement Suspension Matrix at Elevated Temperature. *Polymers*, *14*(11), 2174. https://doi.org/10.3390/polym14112174

gmp Architects. (n.d.). Hyparschale Magdeburg.

Hartig, J. U. (2011). *Numerical investigations on the uniaxial tensile behaviour of Textile Reinforced Concrete* (tech. rep.).

Helbig, T., Unterer, K., Kulas, C., Rempel, S., & Hegger, J. (2016). Fuß- und Radwegbrücke aus Carbonbeton in Albstadt-Ebingen. *Beton- und Stahlbetonbau*, *111*(10), 676–685. https://doi.org/10.1002/best.201600058

Kachkouch, F. Z., Noberto, C. C., de Albuquerque Lima Babadopulos, L. F., Melo, A. R. S., Machado, A. M. L., Sebaibi, N., Boukhelf, F., & El Mendili, Y. (2022). Fatigue behavior of concrete: A literature review on the main relevant parameters. *Construction and Building Materials*, *338*, 127510. https://doi.org/10.1016/j.conbuildmat.2022.127510

Korten, A., & Wetzig, V. (2013). Spalling of concrete – influence of porosity and specimen size and its critical factors regarding safety. *MATEC Web of Conferences*, *6*, 01010. https://doi.org/10.1051/matecconf/20130601010

Peled, A., Mobasher, B., & Bentur, A. (2017). *Textile Reinforced Concrete* (Vol. 19). Taylor & Francis Group.

Sandmann, D., Michler, H., Schumann, A., & Marx, S. (2023, July). STRENGTHENING MONUMENTS WITH TRC. https://doi.org/10.5281/zenodo.8108913

Schneider, K., Michel, A., Liebscher, M., & Mechtcherine, V. (2018). Verbundverhalten mineralisch gebundener und polymergebundener Bewehrungsstrukturen aus Carbonfasern bei Temperaturen bis 500 °C. *Beton- und Stahlbetonbau*, *113*(12), 886–894. https://doi.org/10.1002/best.201800072

Sciegaj, A., Almfeldt, S., Larsson, F., & Lundgren, K. (2023). Textile reinforced concrete members subjected to tension, bending, and in-plane loads: Experimental study and numerical analyses. *Construction and Building Materials*, *408*, 133762. https://doi.org/10.1016/j.conbuildmat.2023.133762

Shihada, S. (2011). Effect of polypropylene fibers on concrete fire resistance. *Journal of Civil Engineering and Management*, *17*(2), 259–264. https://doi.org/10.3846/13923730.2011.574454

Silva, R. M. d. C., Zhao, J., Liebscher, M., Curosu, I., Silva, F. d. A., & Mechtcherine, V. (2022). Bond behavior of polymer- and mineral-impregnated carbon fiber yarns towards concrete matrices at elevated temperature levels. *Cement and Concrete Composites*, *133*, 104685. https://doi.org/10.1016/J.CEMCONCOMP.2022.104685

solidian GmbH. (2024). *solidian GRID Q95-CCE-38 /F01R01) - Technical product data sheet* (tech. rep.). file:///C:/Users/yfe679/Downloads/solidian%20GRID%20Q95-CCE-38%20Technical%20Product%20Data%20Sheet%20v2411.pdf

Solidian-Kelteks. (n.d.-a). Pedestrian Bridge Albstadt Ebingen. https://www.solidian-kelteks.com/en/references/pedestrian-bridge-albstadt-ebingen

Solidian-Kelteks. (n.d.-b). Textile concrete bridge in Albstadt-Lautlingen. https://www.solidian-kelteks.com/en/references/textile-concrete-bridge-in-albstadt-lautlingen

SS-EN-1990. (2014). *SVENSK STANDARD Eurokod-Grundläggande dimensioneringsregler för bärverk Eurocode-Basis of structural design* (tech. rep.). www.sis.se

Suiffi, H., El Maliki, A., Majid, F., & Cherkaoui, O. (2021). The effect of using polypropylene fibers on the durability and fire resistance of concrete. *Frattura ed Integrita Strutturale*, *15*(58), 296–307. https://doi.org/10.3221/IGF-ESIS.58.22

Trafikverket. (2020, March). *250 km/tim med blandad trafik* (tech. rep.). Trafikverket.

Trafikverket. (2021, January). *Krav med rådstext TRVINFRA-00233 - Tunnelbyggande* (tech. rep.).

Trafikverket. (2016, October). *Krav TDOK 2016:0231 Tunnelbyggande* (tech. rep.).

Van Coile, R., Annerel, E., Caspeele, R., & Taerwe, L. (2011). Assessment of the Safety Level of Concrete Slabs during Fire. *Fire Safety Science*, *10*, 1115–1124. https://doi.org/10.3801/IAFFS.FSS.10-1115

Wagner, J., & Curbach, M. (2019). Bond fatigue of TRC with epoxy impregnated carbon textiles. *Applied Sciences (Switzerland)*, *9*(10). https://doi.org/10.3390/app9101980

Williams Portal, N. (2015). *Usability of Textile Reinforced Concrete: Structural Performance, Durability and Sustainability* [Doctoral dissertation, Chalmers University of Technology].

Williams Portal, N., Lohmeyer, R., & Wallbaum, H. (n.d.). *SUSTAINABILITY OF REINFORCEMENT ALTERNATIVES FOR CONCRETE* (tech. rep.).

Xu, S.-l., Shen, L.-h., Wang, J.-y., & Fu, Y. (2014). High temperature mechanical performance and micro interfacial adhesive failure of textile reinforced concrete thin-plate. *Journal of Zhejiang University SCIENCE A*, *15*(1), 31–38. https://doi.org/10.1631/jzus.A1300150

Zhu, D., Liu, H., Rahman, M. Z., Tang, H., & Guo, S. (2024). Fatigue behavior of textile reinforced concrete with different textile types and short steel fiber contents. *Construction and Building Materials*, *443*, 137692. https://doi.org/10.1016/j.conbuildmat.2024.137692

Appendix A. Analytical calculations

Input data

$g = 9.807\ \frac{m}{s^2}$ Acceleration of gravity

Dimensions

$h := 200\ mm$ Thickness/height

$d := 1\ m$ Depth

$b := 1000\ mm$ Width

$u := b = 1\ m$

$A_c := h \cdot b = 0.2\ m^2$ Cross-sectional area

Materials

Concrete C50/60:
Cement N

$\rho_{concrete} := 2550\ \frac{kg}{m^3}$ Density

$f_{ck} := 50\ MPa$ Characteristic compressive strength

$f_{cm} := f_{ck} + 8\ MPa = 58\ MPa$ Average compressive strength

$f_{cd} := \frac{f_{ck}}{1.5} = 33.333\ MPa$

$f_{ctm} := 4.1\ MPa$

Loads

Permanent loads:

$G_k := \rho_{concrete} \cdot g \cdot h \cdot d = 5.001\ \frac{kN}{m}$ Self weight

Support reactions:

$h_{2.1} := 4.4 \cdot m$
$R_{1.1} := 5.15\ m$
$R_{2.1} := 2.8\ m$
$\alpha_1 := 23.8°$
$\beta_1 := 66.2°$

$h_{2.2} := 4.4 \cdot m$
$R_{1.2} := 8.25\ m$
$R_{2.2} := 2.8\ m$
$\alpha_2 := 36°$
$\beta_2 := 54°$

$L_2 := 2 \cdot h_{2.2} + 2 \cdot R_{1.2} \cdot \alpha_2 + 2 \cdot R_{2.2} \cdot \beta_2 = 24.445\ m$ Length of curve for two-track

$V_A := \frac{1.35 \cdot G_k \cdot L_2}{2} = 82.525\ kN$ Support reaction in left support of two-track

Reaction force in one support in FEM-design:

$R_{spring1.1} := 57.65802929\ \frac{kN}{m}$ $L_{spring1.1} := \frac{0.163105}{2}\ m = 0.081553\ m$
$R_{spring1.2} := 53.09393325\ \frac{kN}{m}$ $L_{spring1.2} := L_{spring1.1} = 0.081553\ m$
$R_{spring2.1} := 50.09971697\ \frac{kN}{m}$ $L_{spring2.1} := L_{spring1.1} = 0.081553\ m$
$R_{spring2.2} := 45.74679230\ \frac{kN}{m}$ $L_{spring2.2} := L_{spring1.1} = 0.081553\ m$
$R_{spring3.1} := 42.86425211\ \frac{kN}{m}$ $L_{spring3.1} := L_{spring1.1} = 0.081553\ m$
$R_{spring3.2} := 38.85341259\ \frac{kN}{m}$ $L_{spring3.2} := L_{spring1.1} = 0.081553\ m$
$R_{spring4.1} := 36.19349938\ \frac{kN}{m}$ $L_{spring4.1} := L_{spring1.1} = 0.081553\ m$
$R_{spring4.2} := 32.57510639\ \frac{kN}{m}$ $L_{spring4.2} := L_{spring1.1} = 0.081553\ m$
$R_{spring5.1} := 30.1781212\ \frac{kN}{m}$ $L_{spring5.1} := L_{spring1.1} = 0.081553\ m$
$R_{spring5.2} := 26.94535542\ \frac{kN}{m}$ $L_{spring5.2} := L_{spring1.1} = 0.081553\ m$

$$R_{spring6.1} := 24.80322478 \ \frac{kN}{m} \qquad L_{spring6.1} := L_{spring1.1} = 0.081553 \ m$$

$$R_{spring6.2} := 21.9136082 \ \frac{kN}{m} \qquad L_{spring6.2} := L_{spring1.1} = 0.081553 \ m$$

$$R_{spring7.1} := 19.99056307 \ \frac{kN}{m} \qquad L_{spring7.1} := L_{spring1.1} = 0.081553 \ m$$

$$R_{spring7.2} := 17.38557788 \ \frac{kN}{m} \qquad L_{spring7.2} := L_{spring1.1} = 0.081553 \ m$$

$$R_{spring8.1} := 15.63716006 \ \frac{kN}{m} \qquad L_{spring8.1} := L_{spring1.1} = 0.081553 \ m$$

$$R_{spring8.2} := 13.26011412 \ \frac{kN}{m} \qquad L_{spring8.2} := L_{spring1.1} = 0.081553 \ m$$

$$R_{spring9.1} := 11.65060891 \ \frac{kN}{m} \qquad L_{spring9.1} := L_{spring1.1} = 0.081553 \ m$$

$$R_{spring9.2} := 9.46301371 \ \frac{kN}{m} \qquad L_{spring9.2} := L_{spring1.1} = 0.081553 \ m$$

$$R_{spring10.1} := 7.69973856 \ \frac{kN}{m} \qquad L_{spring10.1} := \frac{0.163127}{2} \ m = 0.081564 \ m$$

$$R_{spring10.2} := 5.70374345 \ \frac{kN}{m} \qquad L_{spring10.2} := L_{spring10.1} = 0.081564 \ m$$

$$k_1 := L_{spring1.1} \cdot R_{spring1.1} + L_{spring1.2} \cdot R_{spring1.2} = 9.032 \ kN$$

$$k_2 := L_{spring2.1} \cdot R_{spring2.1} + L_{spring2.2} \cdot R_{spring2.2} = 7.817 \ kN$$

$$k_3 := L_{spring3.1} \cdot R_{spring3.1} + L_{spring3.2} \cdot R_{spring3.2} = 6.664 \ kN$$

$$k_4 := L_{spring4.1} \cdot R_{spring4.1} + L_{spring4.2} \cdot R_{spring4.2} = 5.608 \ kN$$

$$k_5 := L_{spring5.1} \cdot R_{spring5.1} + L_{spring5.2} \cdot R_{spring5.2} = 4.659 \ kN$$

$$k_6 := L_{spring6.1} \cdot R_{spring6.1} + L_{spring6.2} \cdot R_{spring6.2} = 3.81 \ kN$$

$$k_7 := L_{spring7.1} \cdot R_{spring7.1} + L_{spring7.2} \cdot R_{spring7.2} = 3.048 \ kN$$

$$k_8 := L_{spring8.1} \cdot R_{spring8.1} + L_{spring8.2} \cdot R_{spring8.2} = 2.357 \ kN$$

$$k_9 := L_{spring9.1} \cdot R_{spring9.1} + L_{spring9.2} \cdot R_{spring9.2} = 1.722 \ kN$$

$$k_{10} := L_{spring10.1} \cdot R_{spring10.1} + L_{spring10.2} \cdot R_{spring10.2} = 1.093 \ kN$$

$dz_1 := 0.143701\ m$ $dz_2 := 0.147917$ $dz_3 := 0.151639$
$dx_1 := 0.077158\ m$ $dx_2 := 0.06873$ $dx_3 := 0.060072$

$dz_4 := 0.154856$ $dz_5 := 0.157555$ $dz_6 := 0.159728$
$dx_4 := 0.051214$ $dx_5 := 0.042185$ $dx_6 := 0.033015$

$dz_7 := 0.161369$ $dz_8 := 0.16247$ $dz_9 := 0.163029$
$dx_7 := 0.023735$ $dx_8 := 0.014376$ $dx_9 := 0.004969$

$dz_{10} := 0.163127$
$dx_{10} := 3 \cdot 10^{-6}$

$$\alpha_{spring1} := \operatorname{atan}\left(\frac{dz_1}{dx_1}\right) = 1.078 \qquad \alpha_{spring2} := \operatorname{atan}\left(\frac{dz_2}{dx_2}\right) = 1.136$$

$$\alpha_{spring3} := \operatorname{atan}\left(\frac{dz_3}{dx_3}\right) = 1.194 \qquad \alpha_{spring4} := \operatorname{atan}\left(\frac{dz_4}{dx_4}\right) = 1.251$$

$$\alpha_{spring5} := \operatorname{atan}\left(\frac{dz_5}{dx_5}\right) = 1.309 \qquad \alpha_{spring6} := \operatorname{atan}\left(\frac{dz_6}{dx_6}\right) = 1.367$$

$$\alpha_{spring7} := \operatorname{atan}\left(\frac{dz_7}{dx_7}\right) = 1.425 \qquad \alpha_{spring8} := \operatorname{atan}\left(\frac{dz_8}{dx_8}\right) = 1.483$$

$$\alpha_{spring9} := \operatorname{atan}\left(\frac{dz_9}{dx_9}\right) = 1.54 \qquad \alpha_{spring10} := \operatorname{atan}\left(\frac{dz_{10}}{dx_{10}}\right) = 1.571$$

$V_{spring1} := \cos\left(\alpha_{spring1}\right) \cdot k_1 = 4.273\ kN$

$V_{spring2} := \cos\left(\alpha_{spring2}\right) \cdot k_2 = 3.294\ kN$

$V_{spring3} := \cos\left(\alpha_{spring3}\right) \cdot k_3 = 2.454\ kN$

$V_{spring4} := \cos\left(\alpha_{spring4}\right) \cdot k_4 = 1.761\ kN$

$V_{spring5} := \cos\left(\alpha_{spring5}\right) \cdot k_5 = 1.205\ kN$

$V_{spring6} := \cos\left(\alpha_{spring6}\right) \cdot k_6 = 0.771\ kN$

$V_{spring7} := \cos\left(\alpha_{spring7}\right) \cdot k_7 = 0.444\ kN$

$$V_{spring8} := \cos\left(\alpha_{spring8}\right) \cdot k_8 = 0.208 \ \textbf{kN}$$

$$V_{spring9} := \cos\left(\alpha_{spring9}\right) \cdot k_9 = 0.052 \ \textbf{kN}$$

$$V_{spring10} := \cos\left(\alpha_{spring10}\right) \cdot k_{10} = 0.00002 \ \textbf{kN}$$

$$V_{model.with.springs} := 97.04201 \ \textbf{kN}$$

$$V_{A.model} := V_{model.with.springs} - \begin{pmatrix} V_{spring1} + V_{spring2} + V_{spring3} \\ + V_{spring4} + V_{spring5} + V_{spring6} \\ + V_{spring7} + V_{spring8} + V_{spring9} + V_{spring10} \end{pmatrix} = 82.5803 \ \textbf{kN}$$

$$V_A = 82.52528 \ \textbf{kN}$$

$$\frac{V_{A.model}}{V_A} = 100.066675\%$$

Appendix B. Convergence Study

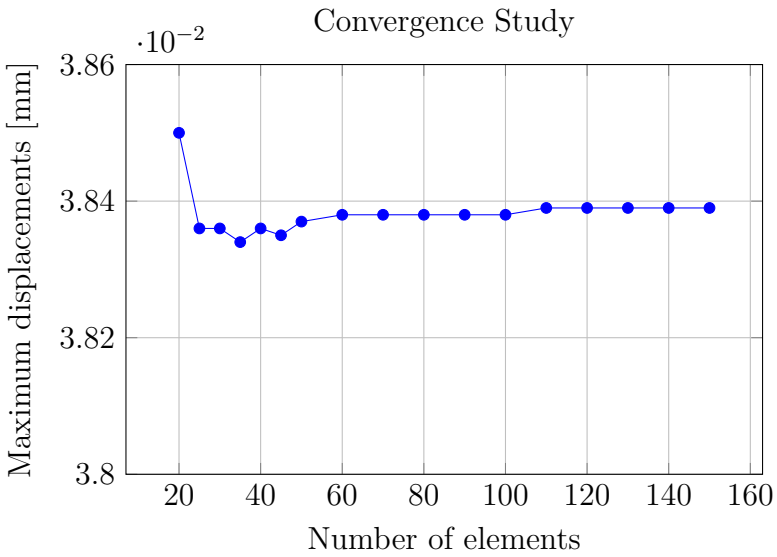

Figure B.1: Convergence study with springs acting in both compression and tension

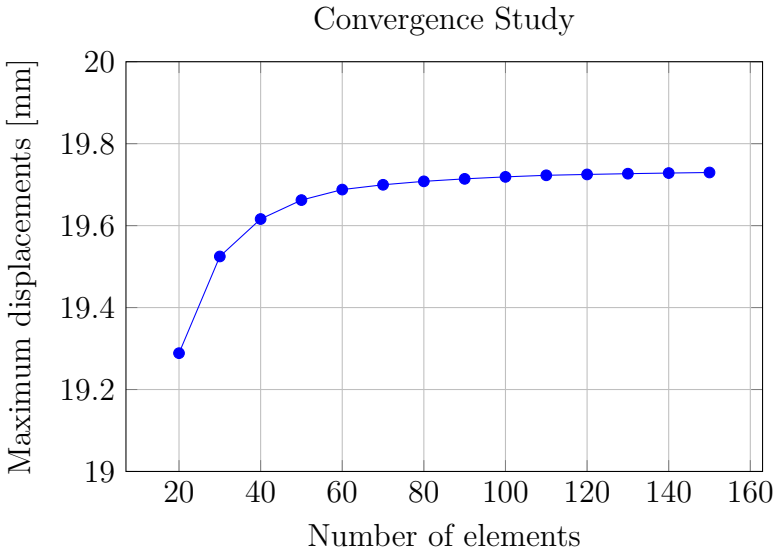

Figure B.2: Convergence study without springs

Appendix C. Design of cross-section RC

Input data

$g = 9.807 \ \frac{m}{s^2}$ — Acceleration of gravity

Dimensions

$h := 130 \ mm$ — Thickness/height

$b := 1000 \ mm$ — Width of one element

$A_c := h \cdot b = 0.13 \ m^2$ — Cross-sectional area

Material properties for concrete C35/45:

Cement N

$\gamma_c := 1.5$ — Partial factor concrete

$\rho_{concrete} := 2550 \ \frac{kg}{m^3}$ — Density

$f_{ck} := 35 \ MPa$ — Characteristic compressive strength

$f_{cm} := f_{ck} + 8 \ MPa = 43 \ MPa$ — Average compressive strength

$f_{cd} := \frac{f_{ck}}{\gamma_c} = 23.333 \ MPa$ — Design compressive strength

$f_{ctm} := 3.2 \ MPa$ — Mean tensile strength

$\varepsilon_{cu} := 0.0035$ — Ultimate compressive strain of concrete

$E_{cm} := 34 \ GPa$ — Youngs modulus of concrete

Material properties for steel B500B:

$\gamma_s := 1.15$ — Partial factor steel

$f_{yk} := 500 \ MPa$ — Characteristic yielding strength

$f_{yd} := \frac{f_{yk}}{\gamma_s} = 435 \ MPa$ — Design yielding strength

$E_s := 200 \ GPa$ — Young's modulus of steel

Dimensioning moment and forces:

Extracted from FEM-design for h=130 mm

$M_{Ed} := 40.8133\ kN \cdot m$ Moment

$N_{Ed} := -32.768\ kN$ Normal force

$V_{Ed} := 35.4684\ kN$ Shear force

Uncracked section

$I_c := \frac{b \cdot h^3}{12} = \left(1.831 \cdot 10^{-4}\right)\ m^4$ Moment of inertia

$z := \frac{h}{2}$ Center of gravity

Flexural tensile strength for concrete according to SS-EN1992-1-1:2005, chapter 3.1.8, eq. 3.23

$k := 1.6 - \frac{h}{1000 \cdot mm} = 1.47$

$f_{ct.fl} := \max\left(k \cdot f_{ctm}, f_{ctm}\right) = 4.704\ MPa$

$\sigma_{cr} := f_{ct.fl}$

$\sigma := \frac{N_{Ed}}{A_c} + \frac{M_{Ed}}{I_c} \cdot z = 14.238\ MPa$

if $\sigma > \sigma_{cr}$
  "Cracks appear"
else
  "No cracks appear"
$=$ "Cracks appear"

Utalization ratio:

$\frac{\sigma}{\sigma_{cr}} = 302.7\%$

Reinforcement needed

Design of cross-section

$M_{Ed} = 40.813\ kN \cdot m$

$N_{Ed} = -32.768\ kN$

$\phi := 16\ mm$ Diameter of steel bars
$\phi' := 8\ mm$

Distance between bars:

Distance between bars according to SS-EN-1992-1-1:2005, chapter 8.2 (2)

$k_{1.rein} := 1$
$k_{2.rein} := 5\ mm$

Maximum grain size of aggregate

$d_g := 22\ mm$

$d_{reinforcement\_min} := \max\left(k_{1.rein} \cdot \phi, d_g + k_{2.rein}, 20\ mm\right) = 27\ mm$

Concrete cover:

Nominal concrete cover according to SS-EN-1992-1-1:2005, chapter 4.4.1.1, eq. 4.1

$c_{nom} = c_{min} + \Delta c_{dev}$

Minimum concrete cover considering adhesion requirements according to SS-EN-1992-1-1:2005, chapter 4.4.1.2 (3)

$c_{min.b} := \phi = 16\ mm$

Minimum concrete cover considering environmental exposure according to BFS 2011:10, section D, table D-1, for L100 and exposure class XC4

$c_{min.dur} := 25\ mm$

Safety allowance according to SS-EN-1992-1-1:2005, chapter 4.4.1.2 (6)

$$\Delta c_{dur.\gamma} := 0 \ mm$$

Minimum concrete cover according to SS-EN-1992-1-1:2005, chapter 4.4.1.2, eq. 4.2

$$c_{min} := \max\left(c_{min.b}, c_{min.dur} + \Delta c_{dur.\gamma}, 10 \ mm\right) = 25 \ mm$$

Allowance for deviation accoring to SS-EN-1992-1-1:2005, chapter 4.4.1.3 (1)

$$\Delta c_{dev} := 10 \ mm$$

$$c_{nom} := c_{min} + \Delta c_{dev} = 35 \ mm$$

Distance from top of cross-section to bottom reinforcement

$$d_1 := h - c_{nom} - \frac{\phi}{2} = 87 \ mm$$

Distance from top of cross-section to top reinforcement

$$d' := c_{nom} + \frac{\phi'}{2} = 39 \ mm$$

Needed cross-section area of steel reinforcement based on moment and normal force

$$A_s := \frac{M_{Ed}}{f_{yd} \cdot 0.9 \cdot d_1} + \frac{-N_{Ed}}{f_{yd}} = 1274.22 \ mm^2$$

Check of the requirement of lower limit of steel cross-section area according to SS-EN-1992-1-1:2005, chapter 9.2.1.1, eq. 9.1N

$$A_{s.min} := 0.26 \cdot \frac{f_{ctm}}{f_{yk}} \cdot b \cdot d_1 = 144.768 \ mm^2$$

$$A_{s.min} := \begin{cases} \text{if } A_{s.min} > 0.0013 \cdot b \cdot d_1 \\ \quad A_{s.min} \\ \text{else} \\ \quad 0.0013 \cdot b \cdot d_1 \end{cases} = 144.768 \ mm^2$$

Check of the requirement of upper limit of steel cross-section area according to SS-EN-1992-1-1:2005, chapter 9.2.1.1 (3)

$A_{s.max} := 0.04 \cdot A_c = 5200\ mm^2$

if $A_{s.min} < A_s < A_{s.max}$ = "OK"
  "OK"
else
  "Not OK"

$n_{drag} := \frac{A_s}{\left(\frac{\phi}{2}\right)^2 \cdot \pi} = 6.337$ Minimum number of bars needed

$n_{tryck} := \frac{A_{s.min}}{\left(\frac{\phi'}{2}\right)^2 \cdot \pi} = 2.88$ Minimum number of bars in compessive zone

$n_{bars} := 7$ $n'_{bars} := 3$ Chosen number of bars

$\beta_R := 0.416$
$\alpha_R := 0.81$ Stress block factors

Minimum distance between bars (chosen)

$d_{reinforcement} := 100\ mm$

Cross-section area of steel reinforcement of chosen number of bars

$A_s := n_{bars} \cdot \left(\frac{\phi}{2}\right)^2 \cdot \pi = 1407.43\ mm^2$

$A'_s := n'_{bars} \cdot \left(\frac{\phi'}{2}\right)^2 \cdot \pi = 150.796\ mm^2$

Vertical space that the reinforcement take compared to the height of the element including the concrete cover

$h_{check} := h - \left(c_{nom} \cdot 2 + \phi + \phi'\right) = 36\ mm$

if $h_{check} > d_{reinforcement\_min}$ = "OK"
  "OK"
else
  "Not OK"

Horisontal space that the reinforcement take compared to the width of the element

$c := c_{nom} \cdot 2 + \phi \cdot n_{bars} + (n_{bars} - 1) \cdot d_{reinforcement} = 782\ mm$ $b = 1000\ mm$

if $c \le b$ = "OK"
  "OK"
else
  "Not OK"

$x := \frac{f_{yd} \cdot A_s}{\alpha_R \cdot f_{cd} \cdot b} = 32.377\ mm$ Height of compressive zone

$\varepsilon_s := \frac{d_1 - x}{x}\ \varepsilon_{cu} = 5.90479 \cdot 10^{-3}$ Strain in steel reinforcement

$\varepsilon_{sy} := \frac{f_{yk}}{E_s} = 0.0025$ Yield strain of steel reinforcement

if $\varepsilon_s > \varepsilon_{sy}$ = "Steel yields"
  "Steel yields"
else
  "Steel does not yield"

Moment capacity of cross-section

$$M_{Rd} := \alpha_R \cdot f_{cd} \cdot b \cdot x \cdot \left(d_1 - \beta_R \cdot x\right) - N_{Ed} \cdot \left(d_1 - \frac{h}{2}\right) = 45.717 \ \boldsymbol{kN \cdot m}$$

$$\text{if } M_{Ed} < M_{Rd} \ = \text{“OK”}$$
$$\quad \| \ \text{“OK”}$$
$$\text{else}$$
$$\quad \| \ \text{“Not OK”}$$

Utilization ratio:

$$\frac{M_{Ed}}{M_{Rd}} = 89.275\%$$

Shear force capacity

Shear slip failure capacity according to SS-EN1992-1-1:2005, chapter 6.2.2:

$$C_{Rd.c} := \frac{0.18}{\gamma_c} = 0.12$$

$$k_{shear} := 1 + \sqrt{\frac{200\ mm}{d_1}} = 2.516$$

$$k_{shear} := \begin{cases} k_{shear} & \text{if } k_{shear} \le 2.0 \\ 2.0 & \text{else} \end{cases} = 2$$

$$\rho_l := \frac{A_s}{b \cdot d_1} = 0.016$$

$$\begin{cases} \text{“OK”} & \text{if } \rho_l \le 0.02 \\ \text{“Not OK”} & \text{else} \end{cases} = \text{“OK”}$$

Shear resistance according to SS-EN1992-1-1:2005, chapter 6.2.2, eq. 6.2.a

$$V_{Rd.c} := \left(C_{Rd.c} \cdot k_{shear} \cdot \left(100 \cdot \rho_l \cdot \frac{f_{ck}}{MPa} \right)^{\frac{1}{3}} \right) MPa \cdot b \cdot d_1 = 80.178\ kN$$

$$v_{min} := 0.035 \cdot k_{shear}^{\frac{3}{2}} \cdot \left(\frac{f_{ck}}{MPa} \right)^{\frac{1}{2}} MPa = 0.586\ MPa$$

$$V_{Rd.c} := \begin{cases} \text{if } V_{Rd.c} > v_{min} \cdot b \cdot d_1 \\ \quad \| \; V_{Rd.c} \\ \text{else} \\ \quad \| \; v_{min} \cdot b \cdot d_1 \end{cases} = 80.178 \ \textbf{kN}$$

Web compression failure capacity according to SS-EN1992-1-1:2005, chapter 6.2.2, eq. 6.5 and 6.6N:

$$v := 0.6 \cdot \left(1 - \frac{f_{ck}}{250 \ \textbf{MPa}}\right) = 0.516$$

$$f_{cd} = 23.333 \ \textbf{MPa}$$

$$V_{Rd.max} := 0.5 \cdot v \cdot f_{cd} \cdot b \cdot d_1 = 523.74 \ \textbf{kN}$$

$$\begin{cases} \text{if } V_{Ed} < V_{Rd.c} \\ \quad \| \; \text{“OK”} \\ \text{else} \\ \quad \| \; \text{“Not OK”} \end{cases} = \text{“OK”} \qquad \begin{cases} \text{if } V_{Ed} < V_{Rd.max} \\ \quad \| \; \text{“OK”} \\ \text{else} \\ \quad \| \; \text{“Not OK”} \end{cases} = \text{“OK”}$$

Crack width

$\phi = 16\ mm$ Reinforcement diameter

$c_{nom} = 35\ mm$ Conrete cover

$h = 130\ mm$ Height of cross-section

$d_1 = 87\ mm$ Distance from top of cross-section to middle of reinforcement

$x = 32.377\ mm$ Height of compressive zone

$A_s = \left(1.407 \cdot 10^3\right)\ mm^2$ Cross-section area of reinforcement

Coefficients according to SS-EN1992-1-1:2005, chapter 7.3.4 (3)

$k_1 := 0.8$ coefficient for bond properties

$k_2 := 0.5$ coefficient for distribution of strain

$k_3 := 3.4$ Recommended value

$k_4 := 0.425$ Recommended value

Effective area of concrete according to SS-EN1992-1-1:2005, chapter 7.3.2 (3)

$h_{c.ef} := min\left(2.5 \cdot \left(h - d_1\right), \frac{\left(h - x\right)}{3}, \frac{h}{2}\right) = 32.541\ mm$ Effective height of cross-section

$A_{c.eff} := h_{c.ef} \cdot b = 0.033\ m^2$ Effective area of concrete

Effective reinforcement ratio according to SS-EN1992-1-1:2005, chapter 7.3.4, eq. 7.10

$$\rho_{\rho.eff} := \frac{A_s}{A_{c.eff}} = 0.043$$

Maximum crack spacing according to SS-EN1992-1-1:2005, chapter 7.3.4, eq. 7.11

$$s_{r.max} := k_3 \cdot c_{nom} + k_1 \cdot k_2 \cdot k_4 \cdot \frac{\phi}{\rho_{\rho.eff}} = 181.889\ mm$$

Cross-section constants Stadium II

$$\alpha := \frac{E_s}{E_{cm}} = 5.882$$

$M_{Ed.quasi} := 23.00\ kN \cdot m$ Moment for quasi-permanet load

$N_{Ed.quasi} := -29.8\ kN$ Normal force for quasi-permanent load

$A_{II} := b \cdot x + \alpha \cdot A_s$

$$x_{tp} := \frac{b \cdot x \cdot \frac{x}{2} + \alpha \cdot A_s \cdot d_1}{A_{II}}$$

$$I_{II} := \frac{b \cdot x^3}{12} + b \cdot x \cdot \left(\frac{x}{2} - x_{tp}\right)^2 + \alpha \cdot A_s \cdot \left(d_1 - x_{tp}\right)^2$$

$x_{guess} := 30\ mm$

$$\sigma_c\left(x_{guess}\right) := \frac{-N_{Ed.quasi}}{A_{II}} + \frac{M_{Ed.quasi}}{I_{II}} \cdot \left(x_{guess} - x_{tp}\right)$$

$x_{II} := \mathbf{root}\left(\sigma_c\left(x_{guess}\right), x_{guess}\right) = 29.465\ mm$

$A_{II} := b \cdot x_{II} + \alpha \cdot A_s = \left(3.774 \cdot 10^4\right)\ mm^2$

$$x_{tp} := \frac{b \cdot x_{II} \cdot \frac{x_{II}}{2} + \alpha \cdot A_s \cdot d_1}{A_{II}} = 30.584\ mm$$

$$I_{II} := \frac{b \cdot {x_{II}}^3}{12} + b \cdot x_{II} \cdot \left(\frac{x_{II}}{2} - x_{tp}\right)^2 + \alpha \cdot A_s \cdot \left(d_1 - x_{tp}\right)^2 = \left(3.589 \cdot 10^7\right)\ mm^4$$

Calculations of steel stress

$z_s := d_1 - x_{tp} = 56.416\ mm$

$$\sigma_c := \frac{-N_{Ed.quasi}}{A_{II}} + \frac{M_{Ed.quasi}}{I_{II}} \cdot z_s = 36.948\ MPa$$

$\sigma_s := \alpha \cdot \sigma_c = 217.341\ MPa$

Difference between mean strain in reinforcement and mean strain in the concrete, according to SS-EN1992-1-1:2005, chapter 7.3.4, eq. 7.9

$k_t := 0.4$ Long term

$$\Delta\varepsilon := \frac{\sigma_s - k_t \cdot \frac{f_{ctm}}{\rho_{\rho.eff}} \cdot \left(1 + \alpha \cdot \rho_{\rho.eff}\right)}{E_s} = 9.011 \cdot 10^{-4}$$

Characteristic crack width w_k according to SS-EN1992-1-1:2005, chapter 7.3.4, eq. 7.8

$w_k := s_{r.max} \cdot \Delta\varepsilon = 0.163897\ mm$

Appendix D. Design of cross-section TRC

Input data

$g = 9.807\ \frac{m}{s^2}$ — Acceleration of gravity

Dimensions

$h := 70\ mm$ — Thickness/height

$b := 1000\ mm$ — Width of one element

$A_c := h \cdot b = 0.07\ m^2$ — Cross-sectional area

Materials properties for concrete C50/60

Cement N

$\gamma_c := 1.5$ — Safety factor concrete

$\rho_{concrete} := 2550\ \frac{kg}{m^3}$ — Density

$f_{ck} := 50\ MPa$ — Characteristic compressive strength

$f_{cm} := f_{ck} + 8\ MPa = 58\ MPa$ — Average compressive strength

$f_{cd} := \frac{f_{ck}}{\gamma_c} = 33.333\ MPa$ — Design compressive strength

$f_{ctm} := 4.1\ MPa$ — Mean compressive strength

$\varepsilon_{cu} := 0.0035$ — Ultimate compressive strain of concrete

Material properties for carbon textile fibres:

$\gamma_{nm} := 1.3$ — Safety factor for fibre textile

$E_0 := 243\ GPa$ — Young's modulus of textile

$\rho_{fibre} := 0.559\ \frac{kg}{m^2}$ — Density of fibres

$f_{nm.k} := 1200\ MPa$ — Characteristic short term tensile strength related to the nominal cross-sectional area

$\eta_f := 0.83$ Efficiency factor

$f_{nm.d} := \frac{f_{nm.k} \cdot \eta_f}{\gamma_{nm}} = 766\ \boldsymbol{MPa}$ Design tenslie strength with an efficiency factor of 0.83

Dimensioning moment and forces:

Extracted from FEM-design for h=120 mm

$M_{Ed} := 25.55\ \boldsymbol{kN \cdot m}$ Moment

$N_{Ed} := -40.9\ \boldsymbol{kN}$ Normal force

$V_{Ed} := 13.0636\ \boldsymbol{kN}$ Shear force

Uncracked section

$I_c := \frac{b \cdot h^3}{12} = \left(2.858 \cdot 10^{-5}\right)\ \boldsymbol{m^4}$ Moment of inertia

$z := \frac{h}{2}$ Center of gravity

Flexural tensile strength for concrete according to SS-EN1992-1-1:2005, chapter 3.1.8, eq. 3.23

$k := 1.6 - \frac{h}{1000 \cdot \boldsymbol{mm}} = 1.53$

$f_{ct.fl} := \max\left(k \cdot f_{ctm}, f_{ctm}\right) = 6.273\ \boldsymbol{MPa}$

$\sigma_{cr} := f_{ct.fl}$

$\sigma := \frac{N_{Ed}}{A_c} + \frac{M_{Ed}}{I_c} \cdot z = 30.701\ \boldsymbol{MPa}$

if $\sigma > \sigma_{cr}$ "Cracks appear"
else "No cracks appear"
$=$ "Cracks appear"

Utalization ratio:

$\frac{\sigma}{\sigma_{cr}} = 489.4\%$

Reinforcement needed

Design of cross-section

$M_{Ed} = 25.55\ \boldsymbol{kN \cdot m}$

$N_{Ed} = -40.9\ \boldsymbol{kN}$

Fibre geometry

$A_{nm} := 8.8\ \boldsymbol{mm^2}$ — Nominal cross-sectional area per fibre strand

$s := 38\ \boldsymbol{mm}$ — Grid width

$a_{nm} := \frac{A_{nm}}{s} = 231.579\ \frac{\boldsymbol{mm^2}}{\boldsymbol{m}}$ — Nominal cross-sectional area per meter

$h_g := 3.3\ \boldsymbol{mm}$ — Grid height

Nominal concrete cover according to SS-EN-1992-1-1:2023, Annex R, chapter R.6

$c := 10\ \boldsymbol{mm}$

Distance from top of cross-section to centre of reinforcement layer

$d_{tex} := h - c - \frac{h_g}{2} = 58.35\ \boldsymbol{mm}$

$z := 0.9 \cdot d_{tex} = 52.515\ \boldsymbol{mm}$ — Lever arm

Needed cross-section area of carbon fibre yarns based on moment and normal force

$A_{tex} := \frac{M_{Ed}}{f_{nm.d} \cdot z} + \frac{-N_{Ed}}{f_{nm.d}} = 688.41\ \boldsymbol{mm^2}$ — Total required reinforcement area

Needed number of yarns

$n_{yarns} := \frac{A_{tex}}{A_{nm}} = 78.228$ — Needed number of yarns

Number of rows of yarns per meter

$n_{rows} := \frac{1\ \boldsymbol{m}}{s} = 26.3158$

Number of layer mesh

$$n_{layers} := \frac{n_{yarns}}{n_{rows}} = 2.973$$

--> 3 layers of mesh is needed for h =70mm

$$n_{layers} := 3$$

Minimum textile reinforcement, taken from DAfStb-Richtlinie

$$A_{tex.min} := 0.6 \cdot \frac{f_{ctm} \cdot b \cdot d_{tex}}{f_{nm.d}} = 187.353 \ mm^2$$

$$\frac{A_{tex.min}}{A_{nm}} = 21.29 \qquad \text{--> 1 layer of mesh}$$

Total area of reinforcement for all 3 layers:

$$A_{tex.tot} := n_{rows} \cdot n_{layers} \cdot A_{nm} = 694.737 \ mm^2$$

Area of reinforcement and distance to mesh:

$A_{tex.1} := n_{rows} \cdot A_{nm} = 231.579 \ mm^2$ Reinforcement area mesh 1

$A_{tex.2} := n_{rows} \cdot A_{nm} = 231.579 \ mm^2$ Reinforcement area mesh 2

$A_{tex.3} := n_{rows} \cdot A_{nm} = 231.579 \ mm^2$ Reinforcfement area mesh 3

$d_{tex.1} := d_{tex} = 58.35 \ mm$ Distance from top to mesh 1

$d_{tex.2} := h - c - h_g - c - \frac{h_g}{2} = 45.05 \ mm$ Distance from top to mesh 2

$d_{tex.3} := h - c - h_g - c - h_g - c - \frac{h_g}{2} = 31.75 \ mm$ Distance from top to mesh 3

Height of compressive zone:

Constraints Guess Values

$$x := \frac{h}{2}$$

$$\alpha \cdot f_{cd} \cdot b \cdot x = E_0 \cdot \eta_f \cdot \left(\frac{d_{tex.1} - x}{x}\right) \cdot \varepsilon_{cu} \cdot A_{tex.1} + E_0 \cdot \eta_f \cdot \left(\frac{d_{tex.2} - x}{x}\right) \cdot \varepsilon_{cu} \cdot A_{tex.2} \hookleftarrow$$
$$+ E_0 \cdot \eta_f \cdot \left(\frac{d_{tex.3} - x}{x}\right) \cdot \varepsilon_{cu} \cdot A_{tex.3}$$

Solver

$$x_{sol} := \mathbf{find}(x) = 44.086 \ mm$$

Check if $\sigma_s < f_{nm.d}$

$$\varepsilon_{s.1} := \left(\frac{d_{tex.1} - x_{sol}}{x_{sol}}\right) \cdot \varepsilon_{cu} = \left(1.132 \cdot 10^{-9}\right) \frac{MPa}{Pa}$$

$$\varepsilon_{s.2} := \left(\frac{d_{tex.2} - x_{sol}}{x_{sol}}\right) \cdot \varepsilon_{cu} = \left(7.653 \cdot 10^{-11}\right) \frac{MPa}{Pa}$$

$$\varepsilon_{s.3} := \left(\frac{x_{sol} - d_{tex.3}}{x_{sol}}\right) \cdot \varepsilon_{cu} = \left(9.794 \cdot 10^{-10}\right) \frac{MPa}{Pa}$$

$\sigma_{s.1} := E_0 \cdot \eta_f \cdot \varepsilon_{s.1} = 228.398\ MPa$

$\sigma_{s.2} := E_0 \cdot \eta_f \cdot \varepsilon_{s.2} = 15.436\ MPa$ $OK!$

$\sigma_{s.3} := E_0 \cdot \eta_f \cdot \varepsilon_{s.3} = 197.527\ MPa$

$f_{nm.d} = 766.154\ MPa$

Distance from top of cross-section of reinforcement area

$$d := \frac{d_{tex.1} \cdot n_{rows} + d_{tex.2} \cdot n_{rows} + d_{tex.3} \cdot n_{rows}}{3 \cdot n_{rows}} = 45.05\ mm$$

$\beta_R := 0.416$ Stress block factors

$\alpha_R := 0.81$

$$M_{Rd} := \alpha_R \cdot f_{cd} \cdot b \cdot x_{sol} \cdot \left(d - \beta_R \cdot x_{sol}\right) - N_{Ed} \cdot \left(d - \frac{h}{2}\right) = 32.205\ kN \cdot m$$

if $M_{Ed} < M_{Rd}$ | = "OK"
 ‖ "OK"
else
 ‖ "Not OK"

Utalization ratio:

$$\frac{M_{Ed}}{M_{Rd}} = 79.336\%$$

Shear force capacity

Shear slip failure capacity according to SS-EN1992-1-1:2005, chapter 6.2.2:

$$C_{Rd.c} := \frac{0.18}{\gamma_c} = 0.12$$

$$k_{shear} := 1 + \sqrt{\frac{200\ mm}{d_{tex}}} = 2.851$$

$$k_{shear} := \begin{cases} \text{if } k_{shear} \le 2.0 \\ \quad k_{shear} \\ \text{else} \\ \quad 2.0 \end{cases} = 2$$

$$\rho_l := \frac{A_{tex}}{b \cdot d_{tex}} = 0.012$$

$$\begin{cases} \text{if } \rho_l \le 0.02 \\ \quad \text{“OK”} \\ \text{else} \\ \quad \text{“Not OK”} \end{cases} = \text{“OK”}$$

Shear resistance according to SS-EN1992-1-1:2005, chapter 6.2.2, eq. 6.2.a

$$V_{Rd.c} := \left(C_{Rd.c} \cdot k_{shear} \cdot \left(100 \cdot \rho_l \cdot \frac{f_{ck}}{MPa} \right)^{\frac{1}{3}} \right) MPa \cdot b \cdot d_{tex} = 54.514\ kN$$

$$v_{min} := 0.035 \cdot k_{shear}^{\frac{3}{2}} \cdot \left(\frac{f_{ck}}{MPa} \right)^{\frac{1}{2}} MPa = 0.7\ MPa$$

$$V_{Rd.c} := \begin{cases} \text{if } V_{Rd.c} > v_{min} \cdot b \cdot d_{tex} \\ \quad V_{Rd.c} \\ \text{else} \\ \quad v_{min} \cdot b \cdot d_{tex} \end{cases} = 54.514\ kN$$

Web compression failure capacity according to SS-EN1992-1-1:2005, chapter 6.2.2, eq. 6.5 and 6.6N:

$$v := 0.6 \cdot \left(1 - \frac{f_{ck}}{250\ \mathit{MPa}}\right) = 0.48$$

$$f_{cd} = 33.333\ \mathit{MPa}$$

$$V_{Rd.max} := 0.5 \cdot v \cdot f_{cd} \cdot b \cdot d_{tex} = 466.8\ \mathit{kN}$$

$$\text{if } V_{Ed} < V_{Rd.c} \mid = \text{“OK”}$$
$$\quad \parallel \text{“OK”}$$
$$\text{else}$$
$$\quad \parallel \text{“Not OK”}$$

$$\text{if } V_{Ed} < V_{Rd.max} \mid = \text{“OK”}$$
$$\quad \parallel \text{“OK”}$$
$$\text{else}$$
$$\quad \parallel \text{“Not OK”}$$

Appendix E. CO_2 calculations

CO_2-eq calculations:

$h_{RC} := 130\ mm$ Height of RC cross-section

$h_{TRC} := 70\ mm$ Height of TRC cross-section

$b := 1000\ mm$ Width of cross-section

$\rho_{concete} := 2550\ \frac{kg}{m^3}$ Density of concrete

$\rho_{steel} := 7850\ \frac{kg}{m^3}$ Density of steel B500B

$\rho_{fibre} := 1300\ \frac{kg}{m^3}$ Density of carbon fibres

$L_1 := 4.35\ m$

$L_2 := 9.901\ m$

$L_3 := 2.933\ m$

$L_{tot} := L_1 \cdot 2 + L_2 + L_3 \cdot 2 = 24.467\ m$

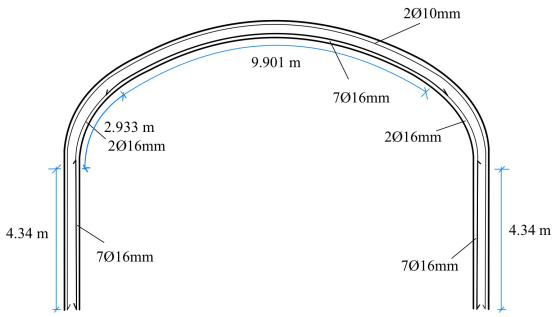

Area of steel and concrete used

Total area of steel reinforcement for 7 ϕ 16mm

$A_{7.16mm} := 1407.43\ mm^2$

Total area of steel reinforcement for 3 ϕ 8mm

$A_{3.8mm} := 150.796\ mm^2$

Total area of textile fibres

$A_{fibres} := 694.737\ mm^2$

Area of concrete for RC cross-section with 7 ϕ 16mm and 3 ϕ 8mm reinforcement

$A_{concrete.RC.7.16mm} := b \cdot h_{RC} - A_{7.16mm} - A_{3.8mm} = 0.128\ m^2$

Area of concrete for RC cross-section with 3 ϕ 8mm in top and bottom

$$A_{concrete.RC.3.8mm} := b \cdot h_{RC} - A_{3.8mm} \cdot 2 = 0.13\ m^2$$

Area of concrete for TRC cross-section

$$A_{concrete.TRC} := b \cdot h_{TRC} = 0.07\ m^2$$

CO_2-eq emission for concrete and reinforcement

CO_2-eq emission for concrete C35/45

$$CO_{2.concrete.C35.45} := 286\ \frac{kg}{m^3}$$

CO_2-eq emission for concrete C50/60

$$CO_{2.concrete.C50.60} := 325\ \frac{kg}{m^3}$$

CO_2-eq emission for steel

$$CO_{2.steel} := 2.3\ \frac{kg}{kg}$$

CO_2-eq emission for carbon fibres

$$CO_{2.fibre} := 19.7\ \frac{kg}{kg}$$

Total CO_2 emission for concrete C35/45

$$CO_{2.eq.tot.concrete.for.RC} := CO_{2.concrete.C35.45} \cdot \begin{pmatrix} A_{concrete.RC.7.16mm} \cdot (2 \cdot L_1 + L_2) \\ + A_{concrete.RC.3.8mm} \cdot 2 \cdot L_3 \end{pmatrix} = 900.888\ kg$$

Total CO_2 emission for concrete C50/60

$$CO_{2.eq.tot.concrete.for.TRC} := CO_{2.concrete.C50.60} \cdot A_{concrete.TRC} \cdot L_{tot} = 556.624\ kg$$

Total CO_2 emission for steel

$$CO_{2.eq.tot.steel} := CO_{2.steel} \cdot \rho_{steel} \cdot \begin{pmatrix} A_{7.16mm} \cdot (2 \cdot L_1 + L_2) \\ + A_{3.8mm} \cdot 2 \cdot L_3 + A_{3.8mm} \cdot L_{tot} \end{pmatrix} = 555.258\ kg$$

Total CO_2 emission for carbon fibres mesh

$$CO_{2.eq.tot.fibres} := CO_{2.fibre} \cdot \rho_{fibre} \cdot A_{fibres} \cdot L_{tot} = 435.322\ kg$$

Total CO_2 emission for RC tunnel lining

$$CO_{2.tot.RC} := CO_{2.eq.tot.concrete.for.RC} + CO_{2.eq.tot.steel} = 1456.146 \ kg$$

Total CO_2 emission for TRC tunnel lining

$$CO_{2.tot.TRC} := CO_{2.eq.tot.concrete.for.TRC} + CO_{2.eq.tot.fibres} = 991.946 \ kg$$

$$\frac{CO_{2.tot.TRC}}{CO_{2.tot.RC}} = 68.121\%$$

$$CO_{2.tot.RC} - CO_{2.tot.TRC} = 464.199 \ kg$$

Appendix F. Maximum moment, normal force and shear force

Table F.1: Maximum positive and negative moment, normal force and shear force for thickness 70 mm

Load combination	**Max positive moment [kNm]**	**Max negative moment [kNm]**	**Normal force [kN]**	**Max shear force [kN]**
LC_1	3.93	-3.7	-21.7	9.30
LC_{2a}	0.47	-0.19	4.94	0.85
LC_{2b}	0.12	-0.10	9.02	0.84
LC_{3a}	23.43	-25.55	-40.90	13.06
LC_{3b}	21.98	-24.88	-44.00	13.64
$LC_{4a.temp.neg}$	22.67	-20.59	-28.20	24.88
$LC_{4a.temp.pos}$	5.02	-8.94	-230	17.78
$LC_{4b.temp.neg}$	22.50	-16.43	-27.3	22.90
$LC_{4b.temp.pos}$	4.39	-10.15	-371	22.36
$LC_{4b.suction.temp.neg}$	22.4	-20.68	-32.5	24.21
$LC_{4b.suction.temp.pos}$	6.58	-10.63	-235	20.98

Table F.2: Maximum positive and negative moment, normal force and shear force for thickness 130 mm

Load combination	**Max positive moment [kNm]**	**Max negative moment [kNm]**	**Normal force [kN]**	**Max shear force [kN]**
LC_1	4.76	-5.28	-39.1	14.00
LC_{2a}	2.44	-1.87	-4.54	5.27
LC_{2b}	0.95	-0.46	5.05	1.33
LC_{3a}	36.59	-39.59	-55.30	19.79
LC_{3b}	33.20	-36.60	-56.00	18.69
$LC_{4a.temp.neg}$	37.87	-24.01	-34.4	31.80
$LC_{4a.temp.pos}$	3.62	-13.65	-345	17.43
$LC_{4b.temp.neg}$	40.81	-13.29	-32.80	35.47
$LC_{4b.temp.pos}$	2.44	-19.29	-562	25.09
$LC_{4b.suction.temp.neg}$	36.53	-22.66	-37.60	32.22
$LC_{4b.suction.temp.pos}$	5.07	-15.03	-345	18.94
SLS	23.00	-2.49	-29.8	14.49

DEPARTMENT ARCHITECTURE AND CIVIL ENGINEERING
CHALMERS UNIVERSITY OF TECHNOLOGY
Gothenburg, Sweden
www.chalmers.se

CHALMERS
UNIVERSITY OF TECHNOLOGY